Biophysical Journal
Article

Biophysical Society

Rupture Dynamics and Chromatin Herniation in Deformed Nuclei

Dan Deviri,[1,*] Dennis E. Discher,[2] and Sam A. Safran[1]
[1]Department of Materials and Interfaces, Weizmann Institute of Science, Rehovot, Israel and [2]Molecular and Cell Biophysics Lab, University of Pennsylvania, Philadelphia, Pennsylvania

ABSTRACT During migration of cells in vivo, in both pathological processes such as cancer metastasis or physiological events such as immune cell migration through tissue, the cells must move through narrow interstitial spaces that can be smaller than the nucleus. This can induce deformation of the nucleus which, according to recent experiments, may result in rupture of the nuclear envelope that can lead to cell death, if not prevented or healed within an appropriate time. The nuclear envelope, which can be modeled as a double lipid bilayer attached to a viscoelastic gel (lamina) whose elasticity and viscosity primarily depend on the lamin composition, may utilize mechanically induced, self-healing mechanisms that allow the hole to be closed after the deformation-induced strains are reduced by leakage of the internal fluid. Here, we present a viscoelastic model of the evolution of a hole nucleated by deformations of the nuclear lamina and estimate the herniation of chromatin through the hole and its relation to the lamin expression levels in the nuclear envelope.

INTRODUCTION

The nucleus of animal cells, which contains the genetic material of the cell in its interior nucleoplasm, is the largest organelle in the cells, with a typical radius of ~ 3 μm in mammalian cells (1,2), and occupies $\sim 10\%$ of the total cell volume (3). The nucleoplasm includes DNA organized into chromatin, dispersed in a small molecule (water/protein/enzyme) solution, which is bounded by the nuclear envelope (NE), comprised of a two-bilayer membrane separated by a volume termed the "perinuclear space". The inner nuclear membrane (INM) is connected to a viscoelastic, dense network of intermediate filament proteins mostly comprising the A- and B-type lamins (the lamina). The INM and the outer nuclear membrane are connected by many nuclear pore complexes (NPCs), containing proteins sometimes modeled as polymer brushes grafted to the inside of cylindrical tubes (4), which results in a protein-covered channel of 50 nm diameter that connects the cytoplasm and the nucleoplasm. The NPC regulates the essential transport of proteins, RNA molecules, and other small ions and molecules to and from the nucleus (5,6); this maintains a controlled environment in the nucleoplasm, distinguished from the cytoplasm, which is essential for proper function of the cell. Because the function of the NE is essential for the survival of the cell, a pathological event that impairs the integrity of the NE may cause an unregulated loss of genetic material and thus lead to cell death.

Recent experiments (7) have shown that motile cells placed on a perforated plate deform as they migrate (within 24 h) from the upper to the lower regions of the plate. However, the migrating cells show a marked reduction in their survival rate as they traverse pores that are smaller than their nucleus size. By using A-type lamin partial knockout cells, it was shown that the survival rate was dependent on the A-type lamin content of the nuclear lamina, which is attached to the INM (8); similar results were obtained in A-type lamin knockout cells subjected to cyclic mechanical strain (9). The composition of the lamina network affects the viscoelastic properties of the NE and the nucleus (10,11), whose rheology obeys power-law scaling: behaving elastically at short times and as a fluid at long times, with no single timescale separating the two regimes (12,13). Migration of cells through narrow constrictions, both in vitro (microfluidic channels) and in vivo (3D collagen networks), may impair the integrity of the NE, resulting in unregulated exchange of cytoplasmic and nucleoplasmic proteins and DNA double-strand breaks, with a probability that increases with decreasing constriction cross section (14,15). Rupture of the NE has not yet been directly imaged in the recently published studies

Submitted January 23, 2017, and accepted for publication July 20, 2017.
*Correspondence: dan.deviri@weizmann.ac.il
Editor: Cecile Sykes.
http://dx.doi.org/10.1016/j.bpj.2017.07.014

and is inferred through observations of the exchange of nucleoplasmic and cytoplasmic proteins (7,14–17). Our predictions for rupture and healing can so far only be correlated with evidence for protein exchange. Evidence of rupture is not unique to migration assays and has also been observed in nuclei squeezed between two parallel surfaces (18). These observations imply that rupture of the NE may be generically caused by deformation-induced, lateral strains and stresses, whose experimental origins may be different. In migration assays, when the constriction dimensions are smaller than the radius of the nucleus, the nucleus must deform for the cells to fit the constriction and migrate. Even in vivo, the NE can support pressure gradients that arise during migration (19); we therefore expect that for relatively small deformations, in the absence of holes, the flow of fluid outside of the nucleus through the NPC must be small so that the nuclear volume is approximately conserved. Shear deformation (deformation that keeps the volume constant) of the undeformed, approximately spherical nucleus in its undeformed state, as shown in Fig. 1 *A*, increases the area of the NE; such area increase results in elastic stretch that leads to surface tensions and strains, which can eventually cause rupture. Interestingly, DNA damage was observed in migrating cells even in the absence of rupture; the damage may be caused by changes in the nucleoplasmic, spatial concentration profile of chromatin that sequester repair enzymes and other essential factors from regions of high chromatin density (16,20).

Understanding and controlling rupture dynamics in vesicles is important for many areas of science, engineering, and medicine such as drug delivery (21), antimicrobial peptides (22), membrane fusion (23), and DNA delivery (24). Due to the importance of the problem, extensive research has been conducted regarding the nucleation and dynamics of pores in fluid, lipid membranes, both in flat membranes (25,26) and in closed vesicles (27–34). However, this body of knowledge disregards the special characteristics of the nucleus, such as its complex internal fluid and viscoelastic membrane. As a result, although migration of cells through interstitial pores in the extracellular matrix is a key characteristic of many biological processes both physiological (embryogenesis, white blood cell migration, wound healing, etc.) and pathological (cancer metastasis or tissue invasion), the mechanism that protects these cells during migration and its fundamental origin is still not well understood.

Measurements of hole formation, growth, and healing, have previously been performed in the context of lipid bilayer vesicles that contain homogenous aqueous solutions. The surface tension was induced not by passage through narrow pores, but by laser tweezers (35) or adhesion (27) (topological changes). In addition, and most importantly, the membrane and internal liquid were fluid in nature and not viscoelastic. A leading hydrodynamic theoretical work on the subject formulated equations describing the dynamics of hole growth and closing coupled to internal fluid leak-out (27,28); numerical solutions of the equations over a wide range of parameters indicated different regimes of the dynamics. In addition, analytical and scaling arguments explaining some of these regimes were presented. Although these studies gave insights into hole formation and dynamics and indeed introduced the concept of outflow of fluid as a controlling factor in hole formation, they were performed in the context of viscous, fluid-filled, lipid vesicles whose properties are different from the NE and chromatin network (36).

The majority (90%) of migration-induced NE rupture events are preceded or coincide with formation and eventual disappearance (probably due to bursting) of nuclear membrane blebs (14). Protein complexes associated with damage response (to bilayers, i.e., ESCRT III proteins that promote bilayers healing and to chromatin, i.e., 53BP1 that binds double-stranded breaks) are recruited after bleb bursting (15). This points to the role of blebs as membrane hole nucleation sites that can then lead to chromatin damage. Disruption of the lamina network, either by lamin knockdown or due to mutations, is positively correlated with the formation of blebs, abnormal nuclear morphology, or impaired nuclear mechanics (18,37,38). This implies a possible mechanistic relation between the integrity of the nuclear lamina and the formation of blebs and subsequent bursting. In this work, we focus on the physics of laminar hole formation and healing, which we assume to be controlled by flow of the lamina; we hypothesize that laminar hole nucleation is an essential first step that must

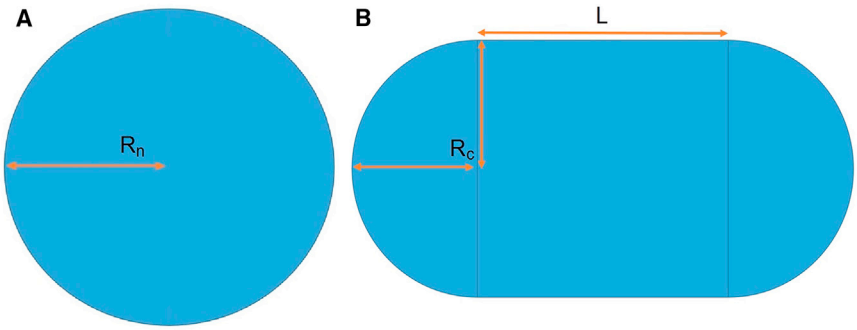

FIGURE 1 Models of the nuclear shape. (*A*) Undeformed state: here we have a sphere of radius R_n and surface area A_u. (*B*) Deformed state: here we show a cylinder of length L and radius R_c (which equals the cross-sectional radius of the constriction when $R_c < R_n$) with two hemispherical caps; the total surface area of the deformed state is A_d. Conservation of the volume of the nucleus determines the length L via the relation $4\pi R_n^3/3 = 4\pi R_c^3/3 + \pi R_c^2 L$. From this, one can find the total area A_d of the deformed nucleus as a function of the constriction cross-sectional radius R_c. To see this figure in color, go online.

precede and then lead to bleb formation, which persists until the laminar hole is healed. However, the physics of bleb formation and bursting is outside the scope of this article, which focuses on lamina hole dynamics/healing and its role in facilitating chromatin extrusion. Our theory thus focuses on the dynamics of rupture in the lamina, which is a crucial first step that precedes bleb formation.

Upon deformation, the internal pressure in the nucleus increases due to the compressive forces exerted on the nucleoplasm. In regions where no external forces are exerted (such as the leading edge), the increased pressure is equilibrated via the Laplace law by the surface tension of the NE. Therefore, the presence of a hole in the lamina (but not the membranes) disrupts the mechanical force balance near the hole. This may lead to fluid outflow from the nucleus that inflates the bilayers in the vicinity of the hole, leading to the formation of a bleb. Once this happens, chromatin normally found in the nucleus can herniate through the lamina hole and then reside in the bleb (14,18). If the bleb bursts, the chromatin may then be damaged due to its exposure to the chemical environment of the cytoplasm. We theoretically predict the dynamics of the lamina ruptures and suggest their biological significance. The molecular properties enter in parameters such as the hole line tension, i.e., lamina 2D Young's modulus E and viscosity η, and the local chromatin-dependent viscosity of the nucleoplasm. (Note that whereas we regard the lamina as compressible within its plane, it is indeed incompressible in three dimensions when its finite thickness is taken into account—namely, stretching in plane leads to a reduction in thickness.)

The theory in this article comprises two subsections: In the first, we formulate and solve what is, to the best of our knowledge, a novel hydrodynamic theory that may describe the postnucleation evolution of the hole radius and lateral strain in the nuclear lamina modeled as a deformed, viscoelastic shell that contains a fluid-filled gel network (as a model of the nucleoplasm) on its lumen side. We analyze this theory analytically in two limits: one in which the deformation-induced strain is relaxed mainly due to outflow; and the other in which strain reduction is mainly due to hole growth. In the second subsection, which is most relevant for the biological problem of chromatin damage, we predict the relative amount of chromatin that herniates through the hole and resides within the forming bleb, as a function of the viscoelastic properties of the lamina. This connects the rupture dynamics predicted by our model and others (28) to biological, rupture-induced damage. Relating the viscoelastic properties of the lamina to the expression of lamins allows prediction of the optimal expression required to prevent significant chromatin herniation, thus optimizing survivability during migration as expected (to some extent) in vivo. These subsections are followed by a discussion that links the theoretical predictions to experimental observation and proposes future experiments to quantitatively test our ideas.

MATERIALS AND METHODS

The theoretical methods of elasticity and hydrodynamics were used to calculate the rupture and healing properties of the lamina. These are detailed in the Supporting Material.

Physical background

The viscoelastic properties of the NE are primarily determined by the nuclear lamina (10,11,13). Various experiments have measured the relative contributions of the different lamin proteins to the mechanical properties of the NE (10,11,37). However, the roles of the different lamins is not yet a matter of consensus, because the varying results and conclusions may depend on the experimental method and the timescales of measurements. In the following sections, where we present and solve the theoretical model, all the predictions are expressed only in terms of the viscosity and 2D Young's modulus of the nuclear envelope. At this level, the theory is generic in nature; the relation between the viscoelastic parameters and the molecular compositions to lamin expression is outside the scope of the theory and must be determined from experiment.

The physics governing area changes in lipid bilayers, which are typically ~4 nm thick (39), is determined by the joint contribution of the elastic forces due to the decrease in the 2D density of lipid molecules (40) and the entropic forces due to suppression of the membranes' thermal undulations (26). Bending moduli of membranes scale as a power law of the membrane thickness (between 2 and 3) (41,42). Because the NE comprises two lipid bilayers and a lamina that is ~14 nm thick (43), it is at least sixfold thicker than lipid bilayers (and may be even thicker because the two lipid bilayers are spaced), and thus has a much larger bending modulus. This effectively suppresses the thermal undulation of the NE and its components and enables the use of purely mechanical, linear elastic constitutive laws when describing the lamina.

Hole formation in flat, tensed membranes, whose molecular area density is lower than its value in a relaxed membrane, results in two opposing contributions to the energy of the membrane: In the first, the hole lowers the membrane energy proportional to its area, due to dispersion, in the rest of the membrane, of the lipid molecules that were originally in the area of the hole. This increases the area density of molecules closer to their equilibrium value and thus reduces the surface deformational energy. In the second, the hole increases the membrane energy in a manner proportional to the hole circumference due to the energy associated with the line tension (29). Line tension promotes hole healing and arises due to the bending energy costs of curving the lipid leaflets on a scale of the order of their thickness, required to eliminate hydrophilic-hydrophobic contact at the circumference of the hole. The competition between line tension and surface tension determines a critical nucleation radius that depends on the deformation-induced surface tension of the membrane; holes smaller than the critical radius will close whereas larger holes will grow up to a characteristic radius (this radius can be metastable (27)). In vesicles comprising only a single lipid bilayer, the time required for the hole formation/healing cycle is of the order of seconds (28), which is much faster than the timescales of migration and rupture measured in migration-induced nuclear rupture (14). Experiments have not yet directly imaged nuclear rupture; so far, existence of rupture was inferred from leakage of nuclear proteins such as GFP-NLS into the cytoplasm (7,14,15,17). Measurements of the time evolution of cytoplasmic fluorescent signal after rupture suggest that the healing of the ruptures occurs on the scale of a few tens of minutes (14,15,17). This time is greatly increased (approximately doubled) by the disruption of the ESCRT III system (15), which indicates its role in the healing of holes in the bleb.

Because the NE contains a variety of integral proteins which, in a coarse-grained picture, can be thought of as defects in a homogeneous viscoelastic layer, it is reasonable to assume that the hole nucleated at such a defect site, such as the NPC. Because the microscopic details of the nucleation are unknown, we consider the growth of a hole whose initial radius is larger

than the critical nucleation radius, and define R_i as the initial hole radius, taken to be 25 nm, of the order of the NPC channel size (5).

The qualitative features of the elastic response of shells, such as the NE, to deformations depends on whether the shells are closed (lack holes with free boundaries) or open (contain holes with free boundaries). Whereas in open shells the boundary of the hole is free to move to reduce the lateral strains, this is not the case in closed shells. Therefore, in open shells, the main contribution to the deformation energy originates in bending of the shell, whereas in closed shells the deformation results in global, in-plane strains (42). Bending involves much smaller deformation energies compared with in-plane strains so that the only large strains in an open shell are those in the direct vicinity of the hole, which cause its growth. In the case of an intact NE, the rigid protein ring formed by NPC can be modeled as a hole with fixed boundaries that cannot relax the imposed surface tension by their motion. Therefore, in its intact state, the NE behaves as a closed shell that is strained (in-plane) over its entire area. On the other hand, rupture of the NE (with the creation of a hole whose size is significantly larger than that of the NPC) creates free boundaries that can adjust to the imposed surface tensions by their motion so that the NE can be modeled as an open shell, in which the lateral strains are concentrated only in the vicinity of the hole. For this reason, we consider only single and not multiple holes in the NE.

Closed surfaces, such as vesicles or the NE, express mechanical equilibrium via the Young-Laplace relation that states that the product of their curvature and surface tension is equal to half the pressure difference between the two sides of the surface. However, once a hole is formed in an otherwise closed membrane, these initial pressure differences lead to an outflow of internal fluid through the hole. This outflow reduces the total area of the surface and hence the packing area per molecule and the surface tension. When the packing area is reduced to its equilibrium packing area that minimizes the membrane free energy value (in the absence of external stress), the surface tension vanishes and along with it, the pressure difference. Previous experiments on the rupture of vesicles, have shown that the two competing mechanisms of surface tension relief (hole growth) and total area reduction (outflow of internal fluid) cause the hole to shrink after an initial period of growth and eliminate the metastable state of the hole that exists in flat membranes (26,27).

However, the nucleoplasm is not a simple viscous fluid (44), and the relation between the flow and pressure gradient is therefore complex. In this article, the nucleoplasm is considered to be a (very) high concentration solution of chromatin fibers in a good solvent (water + small molecules; see Fig. 2 *A*). We model the chromatin as a semiflexible polymer with persistence length l_p. The persistence length of dsDNA in physiological conditions is ~50 nm (45), and we assume that $l_p > 50$ nm due to higher level organization of dsDNA in chromatin fiber. The rheology of the nucleoplasm is considered in two extreme limits, one in which only the aqueous phase can flow (see Fig. 2 *B*) and another, in in which both the chromatin and the aqueous phase flow together (see Fig. 2 *C*). Particle nanotracking experiments have measured an effective, coarse-grained, kinematic viscosity of nucleoplasm that is more than three orders-of-magnitude larger than the kinematic viscosity of water (44), implying that the joint flow of the chromatin and the aqueous phase is considerably more viscous than that of the aqueous phase alone.

RESULTS

Rupture and healing dynamics

In this subsection, we formulate and solve a theory for the coupled dynamics of hole growth/healing of a deformed viscoelastic shell (as a model of the nuclear envelope) and the resulting outflow of a high concentration solution of semiflexible polymer in a good solvent (as a model of chromatin; see Fig. 2 *A*). We consider the postnucleation dynamics of a hole that has been nucleated at a defect site in the shell. High curvature regions in the deformed shell are characterized by higher bending energy; thus, nucleation of holes in regions of high curvature is thermodynamically favorable. We therefore suggest that, for the case of migration-induced deformation, a probable nucleation site of the hole is in the leading edge of the migrating shell because it is characterized by relatively high curvature. Whereas the flow of the solvent phase alone is characterized by a kinematic viscosity η_s, the effect of the semiflexible polymer (which can spatially rearrange during outflow due to friction with the solvent phase) on the rheology of the solution has not yet been elucidated. The friction between the solvent phase and the semiflexible polymer impedes the outflow of the aqueous phase in a manner that may depend on many details.

To account for the unknown, complex effect of the semiflexible polymer on the solvent phase outflow, we consider two very different and simple limiting-case models for the rheology of the solution in our calculations of hole growth and closure. In the first, we consider a scenario in which the semiflexible polymers rearrange such that a channel is formed in between regions where the semiflexible polymers are more densely packed and solvent phase flow is greatly reduced (see Fig. 2 *B*). This channel serves as a conduit

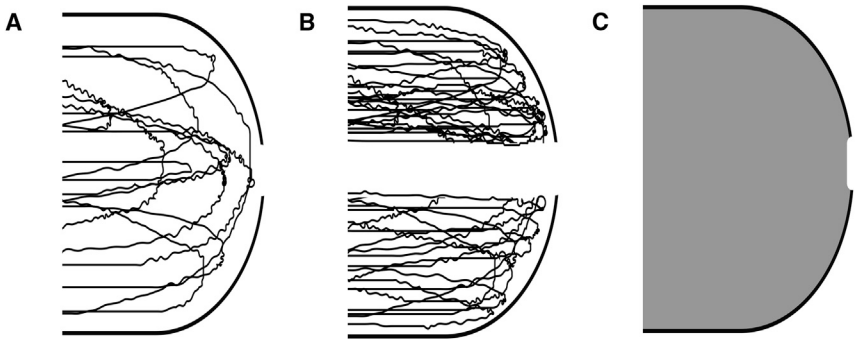

FIGURE 2 Models for chromatin organization and aqueous phase flow. (*A*) Shown here is a high concentration of semiflexible polymer (as a model of chromatin) in a good solvent (water + molecules); the rheology of this model is complex because the polymer chains can rearrange as the solvent phase flows out of the nuclear volume via a hole in the nuclear envelope. (*B*) Limiting case model I: here, polymer chains rearrange (due to the solvent phase flow) to form a channel that serves as a conduit to the solvent phase outflow. The conduit has an effective radius of order of the hole radius R and effective contour length d^*. (*C*) Limiting-case model II: here the polymer and solvent phases flow together and are coarse-grained as a homogenous viscous fluid of viscosity η_s^*.

that directs the flow of the solvent phase and therefore minimizes dissipation by reduction of the friction between the solvent phase and the semiflexible polymers. The flow in the conduit is modeled as a laminar flow in a cylinder (Hagen-Poiseuille flow) whose radius is set by the hole size that allows the solvent phase flow (which is the driving force for the rearrangements of the semiflexible polymers that result in the formation of the channel). The effective tube length can be much larger than the hole size. In the second model, we consider a coarse-grained model of the flow in which the semiflexible polymer phase and the solvent phase are lumped together as a homogenous, viscous fluid with an effective, kinematic viscosity that is much larger than the η_s, the kinematic viscosity of the solvent phase alone (see Fig. 2 *C*). The two models are very different from a physical perspective: in the first model, the semiflexible polymer phase rearranges but does not flow, so that it is distinct from the flowing solvent phase. In the second model, the semiflexible polymer and solvent phases flow together and are treated as a single, homogenous fluid. We show below that, although these two limiting-case models greatly differ, our qualitative predictions for the dependence of the hole growth/healing dynamics and the degree of deformation-induced, polymer extrusion on the viscoelastic properties of the shell are insensitive to which model is used.

Both cases result in similar dynamics that can be approximated by hole growth that increases exponentially with time, until the hole reaches a maximal radius R_m. This regime is followed by an approximately linear decrease of the hole size with time. The major differences between the two models result in different expressions for R_m and the velocity of hole closing (after it reaches its maximum) as functions of the viscoelastic properties of the shell. For this reason, we conclude that the dynamics of an exponential increase, followed by a linear decrease that is common to both models, is insensitive to the details of the effect of the semiflexible polymer phase on the rheology of the solution. We therefore predict that the experimental dynamics of the rupture are of the same form. Below, we show that the qualitative dependence of the amount of polymer that is extruded on the viscoelastic properties of the shell is also independent of the model used for the rheology of the solution. The biological consequences are explicated in the Discussion section at the end of the article, which may be relevant to the reduction in cell viability measured in experiments.

Before deformation and the resulting hole nucleation, the viscoelastic shell is regarded as impermeable and has the shape of a sphere with area A_u (see Fig. 1 *A*). When the spherical shell is deformed, the surface area of the shell increases (because a sphere has minimal area for a fixed volume), laterally stretching the shell. We treat the surface tensions and lateral strains by averaging over the entire area so that the initial strain, ε_0, is proportional to the difference between the areas of the shell in the deformed and undeformed states. (Before hole formation, the NE is approximately impermeable (46), so no outflow occurs.) We account for the rearrangements of the molecules in the shell by an approximately uniform lateral strain driven by the deformation; the timescale for molecular rearrangements in the shell is expected to be much faster than the time for hole growth/healing (tens of minutes), because hole growth/healing involves macroscopic displacements of molecules whereas the rearrangements involve only local displacements at the molecular scale.

Before a hole nucleates, the area of the deformed shell is denoted by A_d; thus, the initial lateral strain ε_0 is given by the difference of the deformed and undeformed areas $\varepsilon_0 = (A_d - A_u)/A_u$. In this article, for geometrical simplicity, we consider deformation of the shell due to forced migration through a constriction. Other deformation mechanisms (e.g., squeezing between plates or others), can in principle be modeled but we focus here on migration due to its biological ubiquity. For the constriction case, we model the deformed shell as a cylinder with two hemispherical caps whose radius is equal to that of the constriction (see Fig. 1 *B*). The geometry in Fig. 1 relates A_d to the constriction cross-sectional area $A_c = \pi {R_c}^2$ by $A_d = (1/3)(4A_c + A_u\sqrt{(A_u/A_c)})$.

The hemispherical, laterally strained caps have smaller radii of curvature and larger surface tension than those of the initial, spherical nucleus. Stabilization of this larger curvature structure implies (via the Young-Laplace relation; Eq. 2) a larger pressure gradient across the shell compared with the initial, undeformed situation. Once a hole is formed, this pressure gradient gives rise to outflow of the solution from the inner side of the shell to the outer side. When hole nucleates, the solvent phase along with some semiflexible polymers flow out through the hole due to this pressure gradient. The importance of this outflow in hole dynamics was previously pointed out in the context of vesicle rupture (27). We note that local changes in the surface tension also contribute to the pressure difference, but our mean field model approximates the surface tension as uniform for the deformations of interest.

The lateral strain ε resulting from the deformation-induced, increased shell area implies surface tension σ; our model uses linear viscoelastic theory (applicable for shell rupture caused by lateral strains of a few percent) to relate the surface tension and lateral strain by $\sigma = E\varepsilon$, where E is the 2D Young's modulus. If the shell is modeled as a Maxwellian, viscoelastic material, the dynamics of its flow and therefore of the hole growth/closing can be complex and dependent on the past configuration of the material. To simplify the problem, we approximate the dynamics of the shell to be solid-like at times that are shorter than the typical viscoelastic timescale $\tau = \eta/E$, where η is the surface viscosity of the shell (which is its kinematic viscosity multiplied by the shell thickness), and viscous fluidlike at times larger than τ. In the solid regime, ignoring plastic

deformations that are usually not relevant for small strains, the material cannot flow, so that the hole radius does not change significantly (see Supporting Material). At times larger than τ, the shell flows as a fluid and its dynamics can be calculated from force balance of the flow around a hole of radius R within a locally flat, viscous layer (see Supporting Material) (27):

$$\frac{dR}{dt} = \frac{1}{2\eta} R\left(\sigma - \frac{T}{R}\right). \tag{1}$$

Equation 1 describes the time evolution of only the hole radius; to predict the full rupture dynamics, an equation for the evolution of the combined area A (defined to be the sum of the shell and the hole area) due to outflow, must be derived. The outflow is driven by a pressure difference Δp between the two sides of the shell; Δp is related to the surface tension by Young-Laplace law,

$$\Delta p = 2\sigma C, \tag{2}$$

where $C = 1/R_c$ is the curvature in the vicinity of the hole (see Fig. 1 *B*). The relation between the flow rate Q of the solvent phase and the pressure difference Δp is different for the two models of the solution rheology considered; we now discuss each of them separately.

Case I: solvent phase flow through a conduit formed by semiflexible polymers

In the first case that we consider (see Fig. 2 *B*), the flow of the solvent phase is modeled as a flow through an effective cylindrical tube of radius R and length d^*, where the dissipation is due to the friction between the flowing solvent phase and the walls of a conduit of contour length d^*, bounded by a dense polymer region where solvent flow is strongly impeded. In this picture, the effective dissipation length d^* can be much larger than R, depending on the contour length of the conduit, which might be very tortuous, leading to d^* that can be greater even than the dimensions of the shell. In this subsection, we formulate and solve a hydrodynamic theory for the dynamics of hole growth and shrinking in the shell for Hagen-Poiseuille outflow.

In the low Reynolds number limit, the outflow is laminar, so that the flow rate Q is (47) (see Supporting Material):

$$Q = -\frac{R_c}{2}\frac{dA}{dt} = \frac{\pi \Delta p R^4}{8\eta_s d^*}, \tag{3}$$

where Δp is the pressure difference between the two sides of the shell, η_s is the viscosity of the solvent phase of the nucleoplasm, and A is the combined area of both the shell and the hole. Equation 3 is accurate in the limit that $d^* >> R$ so that end effects can be neglected.

Substituting linear elasticity relation $\sigma = E\varepsilon$ and Eq. 2 into Eqs. 1 and 3 leads to two coupled equations that describe the dynamics of the combined area of the shell and the local hole radius:

$$\frac{dR}{dt} = \frac{E}{\eta}\frac{R}{2}\left(\varepsilon - \frac{T}{E}\frac{1}{R}\right), \tag{4}$$

$$\frac{dA}{dt} = -\frac{E}{2\eta_s d^*}\frac{\pi^2 R^4}{A_c}\varepsilon. \tag{5}$$

These equations show that the rate of change of the combined area is related to the hole radius by the outflow, whereas the rate of change of the hole radius is related to the lateral strain ε and the line tension T. (The strain is reduced from its initial value by the molecules donated to the shell due to the presence of the hole and by the area reduction due to outflow.)

To simplify the equations, we rescale the variables $\tilde{R}$ and $\tilde{A}$ to be of order unity, i.e., $\tilde{R} = R/R_i$, $\tilde{A} = A/A_u$, and $\tilde{t} = t/\tau$, where $\tau = \eta/E$ and R_i is the initial radius of the hole directly after nucleation. Then, to account for more physical variables, we replace the variable $\tilde{A}$ that appears in Eq. 5 with the lateral strain, which results in the simplified, approximated form (see Supporting Material):

$$\frac{d\tilde{R}}{d\tilde{t}} = \frac{1}{2}\tilde{R}\varepsilon - \frac{\beta}{2}, \tag{6}$$

$$\frac{d\varepsilon}{d\tilde{t}} = -\left(1 + \frac{2\rho\tilde{R}^2}{\delta}\right)\rho\tilde{R}^2\varepsilon + \rho\tilde{R}\beta, \tag{7}$$

where $\varepsilon = (A - \pi R^2 - A_u)/A_u = \tilde{A} - \rho\tilde{R}^2 - 1$ is the dimensionless, small lateral strain; and β, ρ, and δ are small, dimensionless parameters equal to (T/ER_i), $(\pi R_i^2/A_u)$, and $(\eta_s d^*/\eta)$, respectively (see Supporting Material). Henceforth we omit the tilde signs and write R, A, and t.

The dynamical Eqs. 6 and 7 are highly nonlinear and cannot be fully solved analytically. However, some general observations can still be made concerning the dynamics. First ε, which is initially positive, cannot become negative because if ε approaches zero, the derivative in Eq. 7 is dominated by the positive term $\rho\beta R$, which then increases ε. Second, the hole will grow $((dR/dt) > 0)$ up to a maximal size R_m that satisfies $R\varepsilon = \beta$ at the time for which $R = R_m$ as dictated by Eq. 6. Hole growth and outflow decrease ε until it reaches its minimal value (which is shortly after $R = R_m$), because hole closing increases the lateral strain and decreases the outflow. For the minimal strain, the derivative in Eq. 7 is zero and so $\varepsilon_{\min} = (\beta/(1 + (2\rho R^2/\delta))R)$, and the rate of hole closing is then equal to $(dR/dt) = (\beta/2)/(1 + (2\rho R^2/\delta)) - (\beta/2) \approx -(\beta/2)$ $((2\rho R^2/\delta) \gg 1$ for $R \sim R_m$; see Supporting Material), according to Eq. 6.

During hole closing, the lateral strain increases due to the increase of the area outside the hole, which is now occupied by a lower density of molecules because some of those have returned to the previously larger hole. However, that effect is mitigated by outflow from the inner side of the shell that keeps the lateral strain small. If that outflow is large enough, the strain can be maintained at negligibly small values so that Eq. 6 predicts that the hole radius decreases linearly with time. When the effective dissipation length is too high, the outflow is too small to mitigate the growth of the lateral strain by hole closing ($\rho\beta R$ is not small compared to $-2\rho^2/\delta\ R^4\varepsilon$ in Eq. 7), which in turn slows the rate of hole radius decrease. The hole closing rate then returns to the value of $-\beta/2$ when the hole is small enough, because $1/2\ R\varepsilon$ will again be negligible compared with $-\beta/2$ in Eq. 6. Numerical solutions of the equations for a wide range of effective dissipation lengths verify our predictions of the late-time behavior of the hole radius (see Fig. 3).

At early times, before the hole radius reaches its maximal value and then decreases linearly with time, the dynamics is complex and more sensitive to the model parameters. However, one can still qualitatively explain the behavior at early times in two limits:1) fast, outflow-induced strain relaxation compared with hole growth-induced strain relaxation, and 2) for the opposite case. In limit 1, the strain is quickly relieved by outflow whereas the hole size remains approximately constant (or grows very slowly). In that case, the hole radius decreases very soon after the hole forms. In the opposite case of slow outflow (limit 2), the shell combined area is approximately constant as the hole radius increases (due to the surface tension). At early times, when the lateral strain is approximately constant and the constant term in Eq. 6 is negligible, this equation predicts exponential growth of the hole radius as a function of time (28); this can be derived analytically from Eqs. 4 and 5 (see the Supporting Material).

Our numerical analysis of the equations shown in Fig. 3 *A* demonstrates that due to the exponential growth, the maximal hole radius can be significantly greater than the initial hole radius. For biologically relevant values of the parameters (see Supporting Material), we expect $\rho^2/\delta << 1$ but not negligibly small; this supports the assumption that the physical process of hole growth and healing is characterized by the hole-growth-dominated dynamics. In the other limit, $\rho^2/\delta >> 1$, which is

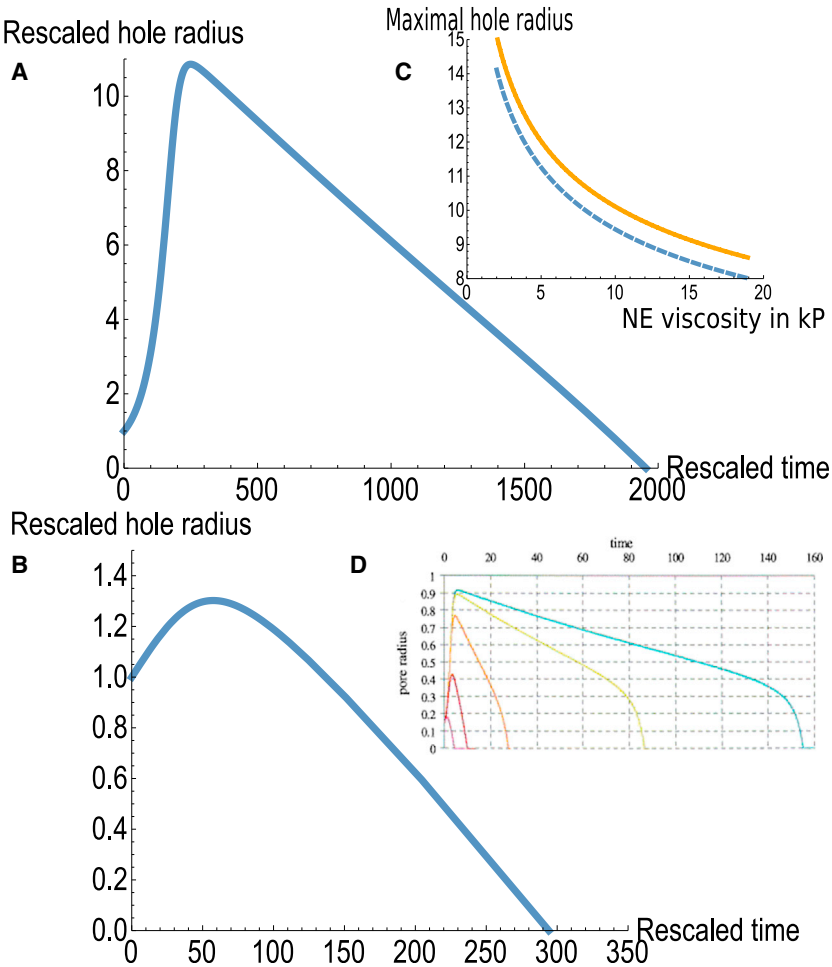

FIGURE 3 Rescaled hole radius R as a function of dimensionless time t for hole-growth-dominated (*A*) and outflow-dominated (*B*) dynamics. (*C*) This shows the maximal hole radius as a function of the shell viscosity numerically (*dashed line*) and analytically, using Eq. 9 (*solid line*). (*D*) Given here is the pore radius as a function of time in rescaled units for increasing inner fluid viscosity from left to right, taken from Brochard-Wyart et al. (28) with permission (fig. 2 in the reference). In (*A–C*), the time is rescaled by the viscoelastic timescale $\tau = \eta/E$, which is estimated to 20 s from the measurements of (10). To see this figure in color, go online.

characterized by either large initial holes or small effective dissipation length d^*, the dynamics of the hole radius are characterized by only a small increase of the hole radius that is quadratic in time. Our numerical analysis of the equations, shown in Fig. 3 *B*, shows that this generally leads to a small increase of the hole radius compared to its initial value before the line tension dominates the physics and the hole begins to shrink. A physical understanding of these two limits is as follows: when d^* is relatively small, the outflow occurs quickly, thus reducing the shell area and relaxing the surface tension induced by the deformation. The hole has then only a relatively short time to grow before the surface tension is reduced and the line tension dominates, causing the hole to shrink. In the other limit, the outflow is much slower and the surface tension is not quickly relaxed, thus permitting the hole to grow to much larger values before the surface tension is relieved and the line tension causes the hole to shrink.

For the purpose of fully characterizing the rupture dynamics (which affects the amount of polymer that extrudes through the hole) in addition to the early and late-time behaviors, one must consider the transition between these two regimes. We thus approximate (see Supporting Material) $R(t)$ as a piecewise function of time, comprising different expressions for growth and healing, where the transition time between the two regimes is denoted by t_m at which the hole reaches its maximum size, R_m.

A closed-form for the maximal radius R_m is given by an expression that can be derived from the dynamical equations (see Supporting Material):

$$2\beta \int_0^{t_m} R^3 dt \approx 1 + \frac{\varepsilon_0 \delta}{\rho^2} - R_m^4. \tag{8}$$

For the case of hole-growth-driven strain-relief dynamics ($(\delta/\rho^2) \gg 1$), we approximate the slope of the linear decrease regime to be $-\beta/2$, and find that (see Supporting Material)

$$R_m \approx \left(\frac{\varepsilon_0 \delta}{\rho^2}\right)^{\frac{1}{4}}, \tag{9}$$

which is in good agreement with the numerics for a wide range of shell surface viscosities, as shown in Fig. 3 *C*.

Equation 9 can be written in dimensional units as $(\pi R_m^2/A_u) = (\varepsilon_0(\eta_s d^*/\eta))^{(1/2)}$, which predicts the ratio of the maximal hole area and the shell undeformed area (for the fixed constriction cross-sectional area). This ratio increases as the square root of the initial strain ε_0, solvent kinematic viscosity η_s, and the effective dissipation length d^*. The value ε_0 is the initial strain that drives hole growth, whereas the strain relief that limits hole growth decreases with increasing η_s or d^*, which limits the outflow and promotes hole growth. The maximal radius also decreases with shell surface viscosity η, which slows the hole growth, thus allowing more strain relief by outflow.

Case II: nucleoplasm as a homogenous viscous fluid

In this case, we coarse-grain the semiflexible polymer and solvent phases and model them both as a homogenous fluid with an effective, kinematic viscosity η_s^*, which is much higher than the kinematic viscosity of the solvent phase alone. In this model, the dissipation length corresponds to the actual thickness of the shell and is therefore typically smaller than the radius of the hole, particularly when the hole size approaches its maximum, the stage at which the outflow is highest and thus most important. This is in contrast to the former case in which d^* was much larger than the hole radius so that the end effects of the flow could be neglected. Here, the inner side of the shell forms a barrier to the flow, which causes bending of the flow lines except in the vicinity of the small hole; this results in an effective dissipation length proportional to R, which leads to a scaling law for Q of the form $Q \sim \Delta p R^3/\eta_s$ (compared with $Q \sim \Delta p R^4/(d^*\eta_s)$ in the former case); a detailed derivation can be found in section 4.29 of (47). This leads to a slightly modified set of equations, which are presented and discussed in the seminal article of the Brochard-Wyart group (28). These equations were solved numerically and analytically in the limit of high internal fluid kinematic viscosity, which is appropriate for the high value of the effective, kinematic viscosity of the solution in this model. The dynamics is characterized by an exponential growth of the hole size up to a maximal hole size, followed by an approximately linear decrease of the hole radius, with a velocity of $(dR/dt) = -(8TdR_m/3\eta_s^* A_u)$ or $(d\tilde{R}/d\tilde{t}) = -(8\beta\rho\tilde{d}/3\pi\delta)\tilde{R}_m$ in dimensionless form (where lengths are rescaled by R_i). The final stage of hole closing is a fast regime with velocity of $-T/2\eta$, similar to the velocity as predicted in the former case (see Fig. 3 *D*).

However, in contrast to the similarities between the dynamics of case I and case II, the maximal hole radius R_m in case II is much larger than that predicted in case I. The ratio of the expressions for outflow of case II and I is $(\eta_s d^*/\eta_s^* R)$ and can be very small if the effective, kinematic viscosity in case II is much larger than the kinematic viscosity of case I, especially for a large hole radius. This implies that the outflow Q in case II is much smaller and is actually negligible in the short, exponentially growing regime in the limit of a large effective, kinematic viscosity of the solution. This means that in this case, the maximal hole radius is the same as the metastable hole radius in flat, tensed membranes (26), and can be written for rescaled dimensionless parameters as (see Supporting Material):

$$R_m = \sqrt{\frac{\varepsilon_0}{\rho}} - \frac{\beta}{2\varepsilon_0}. \tag{10}$$

This is qualitatively different from case I, in which the outflow cannot be neglected in the hole growth regime and serves as a strain relief mechanism that impedes hole growth, leading to a maximal hole radius much smaller than the maximal hole radius of case II. An additional important characteristic of Eq. 10 is that, in contrast to Eq. 9 in the former model, Eq. 10 is independent of the viscoelastic properties of the shell.

Because the fast closing regime is characterized by a hole size that is relatively small, most of the outflow occurs in the slow, approximately linear closing regime (28). Therefore, the fast closing regime is not of any importance in our work; henceforth, we neglect this regime and focus on the slow, approximately linear, closing regime that is the rate-limiting step for hole closing. We shall see in the next subsection that the contribution to the amount of polymer that is extruded through the rupture is primarily determined by this regime.

Polymer extrusion as a model for chromatin herniation

As long as the hole is open, there is a finite probability for a polymer to extrude through the hole. However, this requires the polymer to bend to a radius of curvature that is smaller than the size of the hole. For flow rates that are smaller than $(k_BT/\eta_s) \approx 5(\mu m^3/s)$ (for solvent kinematic viscosity that is comparable to that of water), a condition that is satisfied in systems of biological relevance (see Supporting Material), the bending of the polymer chains is driven by thermal fluctuations (48,49). The rate ν_e of chromatin escape can therefore be written as a sum of Boltzmann factors, and can be approximated by $\nu_e = \nu_0 e^{-(\pi l_p/2R)}$ (where ν_0 is an attempt frequency, and l_p is the persistence length of the semiflexible polymer), which represents the extrusion rate of a polymer chain that is bent to a radius of curvature equal to the maximal radius allowed, the hole radius R, by thermal fluctuation.

To estimate the total amount of polymer that extrudes during a hole growth/healing cycle, which is taken to be exponential growth up to maximal hole radius R_m followed by a linear decrease with a dimensionless, rescaled velocity of $-\alpha$, we integrate ν_e over the entire cycle, which results in the dimensionless measure of the amount of extruded polymer L_c (see the Supporting Material):

$$L_c = \frac{\nu_0 \tau}{\alpha} R_m \left(e^{-\frac{\pi l_p}{2R_m}} + \frac{\pi l_p}{2R_m} \mathrm{Ei}\left(-\frac{\pi l_p}{2R_m} \right) \right), \qquad (11)$$

where τ is the typical viscoelastic timescale η/E of the shell, $\alpha = \beta/2$ for case I, which considers formation of a conduit; and $\alpha = (8\beta\rho d/3\pi\delta)R_m$ for the model of case II, where the entire polymer solution is treated as a high-viscosity, viscous fluid.

Equation 11 is correct for both models of the polymer solution rheology, even though the two models represent completely different approaches to model the complex hydrodynamics of the solution. We therefore conclude that Eq. 11 is universal in the sense that all models for the complex hydrodynamics of the solution will result in expressions of the form of Eq. 11, which differ in the dependences of α and R_m on the model parameters. It is important to note that whereas α appears in the expression for the amount of extruded polymer as a prefactor, R_m appears in the exponent; therefore, changes in R_m affect the amount of extruded polymer much more dramatically than changes of α. This is expected, because the amount of extruded polymer scales linearly with the time that the hole is open, which in turn, approximately scales as $\sim 1/\alpha$, but scales exponentially with the bending energy required to bend the polymer, which scales as $\sim 1/ R_m$ for a maximally sized hole. This also explains why neglecting the fast closing regime of case II is reasonable; the fast closing regime occur for relatively small hole radii, where the amount of extruded polymer is exponentially smaller than the amount for hole radii around R_m. Thus, the amount of extruded polymer is more sensitive to the maximal hole size in the shell than to its closing velocity.

DISCUSSION

We now relate our theory and its predictions to experimental observations of migration-induced rupture and damage. The theory does not depend on the details of the forces applied to the nucleus; what is important is the deformation of the NE that induces stretched, relatively high curvature regions. Thus, many of the results may be applicable to modes of deformation that cause blebbing and rupture other than migration, such as squeezing of the nucleus between two parallel surfaces (18). To apply the theory to these scenarios, the expression for the initial strain and the relation between viscoelastic properties of the NE and the lamins must be revised to account for the new geometry and deformation timescales.

In the scenario we consider, a hole in the lamina (even in the absence of one in the bilayer) is an essential first step that leads to bleb formation and inflation due to outflow, caused by the lack of mechanical force balance across the NE at the site of the laminar hole. The relatively high bending energy of the leading edge can promote nucleation of a hole in the lamina at the leading edge of the cell and nucleus; this prediction is consistent with the experimental observations of the frequent blebbing at the leading edge (8,14,15). We model the process by calculating the dynamics of hole growth and healing and polymer extrusion of a deformed viscoelastic shell that is filled with a high-concentration polymer solution in a good solvent. This model applies to a migrating nucleus where the lamina is treated as a viscoelastic layer and the chromatin as a

semiflexible polymer in a good solvent. Thus, our quantitative predictions focus on the dynamics of growth and healing in the lamina, which is coupled to outflow of fluid from the nucleus, through the hole and into the forming bleb. In addition, we estimate the amount of chromatin that herniates into the bleb as a function of the viscoelastic properties of lamina.

We now discuss possible biophysical implications of hole formation/healing, outflow, and chromatin herniation. These are not explicitly treated by our model but it is interesting to connect our viscoelastic hydrodynamics of the lamina to a possible interpretation of the subsequent processes of biological interest and observations. Although we do not explicitly treat bleb growth, our model is relevant because the growth is driven by outflow of fluid from the nucleoplasm through the lamina hole and into the bleb, eventually causing it to burst, which then transfers chromatin to the cytoplasm. This scenario suggests that the main cause of rupture-associated damage is exposure of chromatin to the cytoplasmic environment, which is biochemically different than the nucleoplasm and may promote chromatin damage. Therefore, the amount of extruded chromatin may correlate with chromatin damage. Of course, it is the bursting of the bleb, not the hole in the lamina, which causes the measured leakage of nucleoplasmic proteins to the cytoplasm; thus, our predictions of the lamina rupture dynamics should not be used to make predictions regarding the leakage of nucleoplasmic proteins, which is experimentally associated with rupture. The hole in the bleb may also heal due to competition between the line tension (which may be effectively augmented by the involvement of the ESCRT system) and the surface tension, which decreases over time due to outflow. We suppose that the time for the healing of holes in the viscoelastic lamina is much longer than the time of bleb formation and bursting. Therefore, we expect multiple cycles of bleb formation and bursting while the hole is open.

To date, experiments have presented qualitative evidence of NE rupture and/or loss of repair enzymes (based mainly on exchange of cytoplasmic and nucleoplasmic proteins), but not direct measurements of the dynamics of hole opening and closing (7,14,15,17). Different cells are characterized by different lamin expression levels and therefore different lamin content of their NE; these molecular-level differences can account for varying viscoelastic properties of the NE (10,11,37). The viscoelastic properties of the lamina control chromatin herniation and as a consequence, nuclear migration-induced damage. Qualitative indications of damage, such as the loss of survivability, chromatin herniation, or double-stranded breaks, were shown to increase with depletion of A-type lamins (8,14).

In addition to hole formation/healing, we have estimated in Eq. 11 the amount of chromatin that herniates through a hole in the lamina and into the bleb; if the bleb subsequently bursts, the chromatin can be transferred into the cytoplasm. Our estimate for herniation (Eq. 11) is presented as a closed form expression depending on two parameters that characterize the dynamics of hole growth and healing: the maximal hole radius R_m and the approximately linear, closing velocity α. The chromatin herniation is predicted to decrease with decreasing R_m or increasing α. However, the contribution of the two do not affect the amount of herniated chromatin in the same manner: whereas the herniation decreases exponentially with R_m, it decreases only inversely with α, which appears as a prefactor in Eq. 11. The parameters R_m and α are determined by the line tension T, which is proportional to the 2D Young's modulus E (see Supporting Material), and the surface viscosity of the lamina η; however, the exact dependence of R_m and α on the viscoelastic parameters η and E is sensitive to the rheology of the nucleoplasm. In our model, we predict that R_m decreases with increasing η but is independent of E, whereas α decreases with η and increases with E.

An increase of the lamina surface viscosity η slows the 2D flows within the lamina and retards hole growth. This retardation means that a relatively large amount of nucleoplasm can flow out of the hole leading to additional strain relief, compared with a system in which the hole grows quickly, so that the change of nuclear volume during hole growth is minimal. Thus, an increase of the surface viscosity of the lamina reduces the maximal hole radius, at least for case I of the rheology that we considered above. Because chromatin herniation is exponentially sensitive to the hole radius, our predicted decrease of R_m with increasing lamina surface viscosity (for one of the rheological models) means that increasing the laminar viscosity should greatly reduce the chromatin herniation.

Conversely, an increase of the 2D Young's modulus E, which controls the line tension responsible for hole closing, does not considerably modify the maximal hole radius. For large holes, the force due to line tension is inversely proportional to the hole radius and thus negligible compared with the surface tension. The line tension is thus relevant only after the surface tension becomes relaxed, at the hole closing regime. Indeed, in both models of the nuclear rheology the maximal hole radius is approximately independent of the line tension T. However, the line tension does affect the hole closing rate because the line tension is the driving force for the healing process. Indeed, the hole closing velocity, α, increases with T. Thus, increasing the laminar elastic modulus, E, will lead to an increase of α and to a decrease in the herniation of chromatin. In contrast to an increase in the laminar viscosity, which leads to a possibly exponential decrease of the herniation, an increase of E algebraically decreases the herniation because it enters through the prefactor and not the exponent.

Various experiments have measured the relative contributions of the different lamin subtypes to the viscoelastic properties of the NE. These experiments, which differed in the timescales and method of measurements, have been interpreted to ascribe differing contributions of A-type lamins

to the viscoelastic properties. In some experiments, A-type lamins were found to contribute primarily to the viscosity η (10,50), whereas in others it was found to contribute to the stiffness (11,37). Our predictions for chromatin herniation summarized here are cast in terms of the viscoelastic parameters and future experiments elucidating their molecular origins at the timescales appropriate to laminar hole formation/closing will enable further understanding at the molecular scale.

Returning to the focus of our theory, we suggest the following experiments. First, quantitative imaging of the lamina hole size as a function of the viscoelastic properties of the NE can distinguish between the two models we presented for the nucleoplasm rheology and determine which is more realistic. For example, measurements of the maximal hole radius R_m, as a function of the NE surface viscosity η, can distinguish the conduit model (case I) from the homogeneous viscous fluid model (case II), because Eq. 9 for case I predicts $R_m \sim \eta^{-1/4}$, whereas Eq. 10 for R_m (case II) is independent of η. Similar quantification can be done for the velocity of hole closing in regime where the velocity is approximately constant. In addition, quantification of chromatin herniation as a function of R_m or α, by quantitative imaging of the hole size as a function of time, can test Eq. 11 for chromatin herniation. Quantification of the amount of chromatin that herniates through the hole as a function of the A-type lamin expression levels should also allow experiments to distinguish between the proposed contributions of type-A lamins to the viscoelastic properties of the lamina: if expression of type-A lamins mainly augments the viscosity, one might observe an exponential change of the chromatin herniation, whereas if it mainly augments the stiffness (through increasing E), we predict a possibly weaker algebraic dependence.

SUPPORTING MATERIAL

Supporting Materials and Methods are available at http://www.biophysj.org/biophysj/supplemental/S0006-3495(17)30812-3.

AUTHOR CONTRIBUTIONS

D.D. performed research and wrote the article. D.E.D. designed research and contributed to the article. S.A.S. designed research and wrote the article.

ACKNOWLEDGMENTS

The authors thank F. Brochard-Wyart, B. Berkowitz, J. Karni, R. Bar-Ziv, Y. Garini, M. Lenz, D. Ben-Yaakov, J. Irianto, C. Pfeifer, Y. Xia, K. Wolf, J. Lammerding, O. Cohen, and A. Moriel for the enlightening comments and useful discussions.

This work was funded by the U.S.-Israel Binational Science Foundation and the Israel Science Foundation, and was supported by the Schmidt Minerva Center and the Villalon Foundation. The historic generosity of the Perlman Family Foundation is also acknowledged.

REFERENCES

1. Li, G. W., and X. S. Xie. 2011. Central dogma at the single-molecule level in living cells. *Nature.* 475:308–315.
2. Phillips, R., J. Kondev, …, H. Garcia. 2012. Physical Biology of the Cell. Garland Science, New York.
3. Alberts, B., A. Johnson, …, P. Walter. 2002. Molecular Biology of the Cell. Garland Science, New York.
4. Photos, P. J., H. Bermudez, …, D. E. Discher. 2007. Nuclear pores and membrane holes: generic models for confined chains and entropic barriers in pore stabilization. *Soft Matter.* 3:364–371.
5. Grossman, E., O. Medalia, and M. Zwerger. 2012. Functional architecture of the nuclear pore complex. *Annu. Rev. Biophys.* 41:557–584.
6. Burke, B., and C. L. Stewart. 2014. Functional architecture of the cell's nucleus in development, aging, and disease. *Curr. Top. Dev. Biol.* 109:1–52.
7. Irianto, J., R. Charlotte, …, D. E. Discher. 2015. Constricted cell migration causes nuclear lamina damage, DNA breaks, and squeeze-out of repair factors. *bioRxiv.* http://dx.doi.org/10.1101/035626.
8. Harada, T., J. Swift, …, D. E. Discher. 2014. Nuclear lamin stiffness is a barrier to 3D migration, but softness can limit survival. *J. Cell Biol.* 204:669–682.
9. Lammerding, J., P. C. Schulze, …, R. T. Lee. 2004. Lamin A/C deficiency causes defective nuclear mechanics and mechanotransduction. *J. Clin. Invest.* 113:370–378.
10. Swift, J., I. L. Ivanovska, …, D. E. Discher. 2013. Nuclear lamin-A scales with tissue stiffness and enhances matrix-directed differentiation. *Science.* 341:1240104.
11. Stephens, A. D., E. J. Banigan, …, J. F. Marko. 2017. Chromatin and lamin A determine two different mechanical response regimes of the cell nucleus. *Mol. Biol. Cell.* 28:1984–1996.
12. Christensen, R. 2012. Theory of Viscoelasticity: An Introduction. Elsevier, Dordrecht, Netherlands.
13. Dahl, K. N., A. J. Engler, …, D. E. Discher. 2005. Power-law rheology of isolated nuclei with deformation mapping of nuclear substructures. *Biophys. J.* 89:2855–2864.
14. Denais, C. M., R. M. Gilbert, …, J. Lammerding. 2016. Nuclear envelope rupture and repair during cancer cell migration. *Science.* 352:353–358.
15. Raab, M., M. Gentili, …, M. Piel. 2016. ESCRT III repairs nuclear envelope ruptures during cell migration to limit DNA damage and cell death. *Science.* 352:359–362.
16. Irianto, J., C. R. Pfeifer, …, D. E. Discher. 2016. Nuclear constriction segregates mobile nuclear proteins away from chromatin. *Mol. Biol. Cell.* 27:4011–4020.
17. Robijns, J., F. Molenberghs, …, T. D. J. Corne. 2016. In silico synchronization reveals regulators of nuclear ruptures in lamin A/C deficient model cells. *Sci. Rep.* 6:30325.
18. Le Berre, M., J. Aubertin, and M. Piel. 2012. Fine control of nuclear confinement identifies a threshold deformation leading to lamina rupture and induction of specific genes. *Integr. Biol.* 4:1406–1414.
19. Ryan, J., H. K. Petrie, and K. M. Yamada. 2014. Generation of compartmentalized pressure by a nuclear piston governs cell motility in a 3D matrix. *Science.* 345:1062–1065.
20. Bennett, R. R., C. R. Pfeifer, …, A. J. Liu. 2017. Elastic-fluid model for DNA damage and mutation from nuclear fluid segregation due to cell migration. *Biophys. J.* 112:2271–2279.
21. Schroeder, A., J. Kost, and Y. Barenholz. 2009. Ultrasound, liposomes, and drug delivery: principles for using ultrasound to control the release of drugs from liposomes. *Chem. Phys. Lipids.* 162:1–16.
22. Huang, H. W. 2006. Molecular mechanism of antimicrobial peptides: the origin of cooperativity. *Biochim. Biophys. Acta Biomembr.* 1758:1292–1302.
23. Kozlovsky, Y., L. V. Chernomordik, and M. M. Kozlov. 2002. Lipid intermediates in membrane fusion: formation, structure, and decay of hemifusion diaphragm. *Biophys. J.* 83:2634–2651.

24. Smith, K. C., J. C. Neu, and W. Krassowska. 2004. Model of creation and evolution of stable electropores for DNA delivery. *Biophys. J.* 86:2813–2826.
25. Safran, S. A., and J. Klein. 1993. Surface instability of viscoelastic thin films. *J. Phys. II.* 3:749–757.
26. Sens, P., and S. A. Safran. 1998. Pore formation and area exchange in tense membranes. *Eur. Phys. Lett.* 43:95.
27. Sandre, O., L. Moreaux, and F. Brochard-Wyart. 1999. Dynamics of transient pores in stretched vesicles. *Proc. Natl. Acad. Sci. USA.* 96:10591–10596.
28. Brochard-Wyart, F., P. G. De Gennes, and O. Sandre. 2000. Transient pores in stretched vesicles: role of leak-out. *Phys. A.* 278:32–51.
29. Levin, Y., and M. A. Idiart. 2004. Pore dynamics of osmotically stressed vesicles. *Phys. A.* 331:571–578.
30. Idiart, M. A., and Y. Levin. 2004. Rupture of a liposomal vesicle. *Phys. Rev. E Stat. Nonlin. Soft Matter Phys.* 69:061922.
31. Ryham, R. J., F. S. Cohen, and R. S. Eisenberg. 2012. A dynamic model of open vesicles in fluids. *Commun. Math. Sci.* 10:1273–1285.
32. Ryham, R., I. Berezovik, and F. S. Cohen. 2011. Aqueous viscosity is the primary source of friction in lipidic pore dynamics. *Biophys. J.* 101:2929–2938.
33. Gozen, I., and P. Dommersnes. 2014. Pore dynamics in lipid membranes. *Eur. Phys. J. Spec. Top.* 223:1813–1829.
34. Fan, H., Y. Chen, and K. Y. Sze. 2009. Phenomenological modeling for pore opening, closure and rupture of the GUV membrane. *Int. J. Appl. Mech.* 1:327–338.
35. Bar-Ziv, R., E. Moses, and P. Nelson. 1998. Dynamic excitations in membranes induced by optical tweezers. *Biophys. J.* 75:294–320.
36. Bronshtein, I., I. Kanter, …, Y. Garini. 2016. Exploring chromatin organization mechanisms through its dynamic properties. *Nucleus.* 7:27–33.
37. Lammerding, J., L. G. Fong, and R. T. Lee. 2006. Lamins A and C but not lamin B1 regulate nuclear mechanics. *J. Biol. Chem.* 281:25768–25780.
38. Dahl, K. N., A. J. Ribeiro, and J. Lammerding. 2008. Nuclear shape, mechanics, and mechanotransduction. *Circ. Res.* 102:1307–1318.
39. Mitra, K., I. Ubarretxena-Belandia, …, D. M. Engelman. 2004. Modulation of the bilayer thickness of exocytic pathway membranes by membrane proteins rather than cholesterol. *Proc. Natl. Acad. Sci. USA.* 101:4083–4088.
40. Safran, S. A. 1994. Statistical Thermodynamics of Surfaces, Interfaces, and Membranes, Vol. 90. Perseus, New York.
41. Safran, S. A. 1999. Curvature elasticity of thin films. *Adv. Phys.* 48:395–448.
42. Landau, L. D., and E. M. Lifshitz. 1986. Theory of Elasticity, Vol. 7, Course of Theoretical Physics, 3. Butterworth-Heinemann, Oxford, UK, p. 109.
43. Turgay, Y., M. Eibauer, …, O. Medalia. 2017. The molecular architecture of lamins in somatic cells. *Nature.* 543:261–264.
44. Tseng, Y., J. S. Lee, …, D. Wirtz. 2004. Micro-organization and viscoelasticity of the interphase nucleus revealed by particle nanotracking. *J. Cell Sci.* 117:2159–2167.
45. Bustamante, C., S. B. Smith, …, D. Smith. 2000. Single-molecule studies of DNA mechanics. *Curr. Opin. Struct. Biol.* 10:279–285.
46. Neelam, S., T. J. Chancellor, …, T. P. Lele. 2015. Direct force probe reveals the mechanics of nuclear homeostasis in the mammalian cell. *Proc. Natl. Acad. Sci. USA.* 112:5720–5725.
47. Happel, J., and H. Brenner. 2012. Low Reynolds Number Hydrodynamics: With Special Applications to Particulate Media, Vol. 1. Springer Science & Business Media, New York.
48. Daoudi, S., and F. Brochard. 1978. Flows of flexible polymer solutions in pores. *Macromolecules.* 11:751–758.
49. Béguin, L., B. Grassl, …, H. Duval. 2011. Suction of hydrosoluble polymers into nanopores. *Soft Matter.* 7:96–103.
50. Pajerowski, J. D., K. N. Dahl, …, D. E. Discher. 2007. Physical plasticity of the nucleus in stem cell differentiation. *Proc. Natl. Acad. Sci. USA.* 104:15619–15624.

Biophysical Journal, Volume *113*

Supplemental Information

Rupture Dynamics and Chromatin Herniation in Deformed Nuclei

Dan Deviri, Dennis E. Discher, and Sam A. Safran

Rupture dynamics and chromatin herniation in deformed nuclei

Dan Deviri[1], Dennis E. Discher[2], and Sam A. Safran[1]

[1]Department of Materials and Interfaces, Weizmann Institute of Science, Rehovet 76100, Israel

[2]Molecular and Cell Biophysics Lab, University of Pennsylvania, Philadelphia, Pennsylvania 19104

Supplementary material

Elastic deformation of the hole

Here, we show that in the elastic regime, the hole radius does not appreciably change from its initial radius. For times that are shorter than the typical viscoelastic timescale $\tau = E/\eta$, the change in the hole radius is governed by linear elasticity. For approximately flat shells, this is a problem of a two-dimensional annulus with boundary conditions of constant stress $\tilde{\sigma}_0$ that equals $\tilde{E}\varepsilon_0$ at infinity, where $\tilde{E}$ is the three-dimensional Young's modulus (E is the two-dimensional Young's modulus, which is related to $\tilde{E}$ by $E \sim \tilde{E} \cdot d$ where d is the shell thickness), and a size dependent line tension of the hole on the perimeter of the annulus. Force balance dictates

$$\frac{\partial \tilde{\sigma}_{rr}}{\partial r} + \frac{1}{r}\left(\tilde{\sigma}_{rr} - \tilde{\sigma}_{\theta\theta}\right) = 0 \tag{1}$$

where $\tilde{\sigma}_{ij}$ is the component of the stress tensor. In linear elasticity the stresses and strains are related by

$$\tilde{\sigma}_{ij} = \frac{\tilde{E}}{1+\nu}\left(\varepsilon_{ij} + \frac{\nu}{1-2\nu} tr\left(\varepsilon\right)\delta_{ij}\right) \tag{2}$$

where ε_{ij} are the components of the strain tensor and ν is the Poisson ratio. We work in a coordinate system in which the $\hat{z}$ axis is the symmetry axis of the annulus and $z = 0$ characterizes the midplane of the shell. From symmetry considerations, the θ component of the displacement vector $\vec{u}$ vanishes while other components are θ independent. This means that $\varepsilon_{rr} = \frac{\partial u_r}{\partial r}, \varepsilon_{\theta\theta} = \frac{u_r}{r}, \varepsilon_{zz} = \frac{\partial u_z}{\partial z}$ and $\varepsilon_{rz} = \frac{1}{2}\left(\frac{\partial u_r}{\partial z} + \frac{\partial u_z}{\partial r}\right)$ while all other components vanish.

The upper and lower surfaces of the shell are traction free. This means, for a thin shell, that all the components of $\tilde{\sigma}_{iz}$ can be approximated to be zero, in particular $\tilde{\sigma}_{zz} = 0$ which gives, using Eq. 2 and the relations between the strain and displacement components, $\varepsilon_{zz} = -\frac{\nu}{1-\nu}\left(\frac{\partial u_r}{\partial r} + \frac{u_r}{r}\right)$. Substituting this into Eq. 2 together with the relation between the strain and displacement components leads to:

$$\tilde{\sigma}_{rr} = \frac{\tilde{E}}{1+\nu}\left(\frac{\partial u_r}{\partial r} + \frac{\nu}{1-\nu}\left(\frac{\partial u_r}{\partial r} + \frac{u_r}{r}\right)\right) \tag{3}$$

$$\tilde{\sigma}_{\theta\theta} = \frac{\tilde{E}}{1+\nu}\left(\frac{u_r}{r} + \frac{\nu}{1-\nu}\left(\frac{\partial u_r}{\partial r} + \frac{u_r}{r}\right)\right) \tag{4}$$

Substituting these relations into Eq. 1 gives the differential equation

$$\frac{\partial^2 u_r}{\partial r^2} + \frac{1}{r}\frac{\partial u_r}{\partial r} - \frac{u_r}{r^2} = 0 \tag{5}$$

whose solution is

$$u_r = Ar + B\frac{1}{r} \tag{6}$$

where A and B are integration constants determined by the boundary conditions $\tilde{\sigma}_{rr}(r \to \infty) = \tilde{\sigma}_0$ and $d \cdot \tilde{\sigma}_{rr}(r = R_i) = \frac{T}{R_i}$. Using equations 6 and 3 allow us to express the radial component of the stress tensor as a function of r and the integration constants:

$$\tilde{\sigma}_{rr}(r) = \frac{\tilde{E}}{1+\nu}\left(\frac{1+\nu}{1-\nu}A - B\frac{1}{r^2}\right) \tag{7}$$

The expression above, together with the stress boundary conditions determines $A = \frac{(1-\nu)\tilde{\sigma}_0}{\tilde{E}}$ and $B = \frac{1+\nu}{\tilde{E}}R_i^2\tilde{\sigma}_0 - \frac{1+\nu}{\tilde{E}}\frac{R_i T}{d}$. Substituting the integration constants A and B into 6 with $R = R_i$ results in the displacement of the hole $u_r(r = R_i) = 2R_i\frac{\tilde{\sigma}_0}{\tilde{E}} - (1+\nu)\frac{T}{d\cdot\tilde{E}}$. In linear elasticity $T/d, \tilde{\sigma}_0 \ll \tilde{E}$, so that the change in the hole radius is negligible compared with the radius itself. We therefore conclude that in the short-time elastic regime, the hole radius is essentially unchanged for times smaller than the typical viscoelastic timescale τ, where the shell is approximated to respond elastically.

Derivation of the dynamical equations

To formulate the equations for the hole dynamics in case I, we have to account for the flow of the shell, the high-concentration, polymer solution and their coupling. We consider each of these in separate subsections.

Shell flow dynamics

For times larger than the typical viscoelastic timescale $\tau = \eta/E$, the shell flow is controlled by low Reynolds number hydrodynamics. We approximate the shell to be a three-dimensional incompressible, viscous thin film with a hole of radius R. The boundary conditions are: surface tension σ equals $E\varepsilon$ at infinity and an equivalent surface tension of $T/R(t)$ that arises from the line tension and the time dependent hole radius; the upper and lower surfaces of the film are traction free. We again work in a coordinate system in which the $\hat{z}$ axis is the symmetry axis of the annulus and $z = 0$ characterizes the midplane of the shell. Symmetry considerations dictate, that the θ component of the velocity field $\vec{v}$ of the shell vanishes and that v_r and v_z are θ independent. Using these symmetry arguments, the incompressibility condition is written as:

$$\nabla \cdot \vec{v}(r,t) \;=\; \frac{1}{r}\frac{\partial (r v_r)}{\partial r} + \frac{\partial v_z}{\partial z} = 0 \tag{8}$$

For a thin shell, the flow of the molecules is quasi two-dimensional in the plane of the shell while the change in its thickness is governed by its three-dimensional incompressibility. Thus, changes in the molecular rearrangements in the z direction occur almost instantaneously; v_z and its derivatives are therefore very small compared with their corresponding quantities in the radial direction.

Eq. 8 is therefore well approximated by $\frac{1}{r}\frac{\partial (r v_r)}{\partial r} = 0$, therefore $v_r = G(t,z)/r$. Since the upper and lower surfaces are traction free, the hydrodynamic stress tensor $\tilde{\sigma}_{zr}$ vanishes on both surfaces. For a thin shell, this means that $\tilde{\sigma}_{zr}$ is approximately zero throughout the thickness of the shell: $\tilde{\sigma}_{zr} = \tilde{\eta}\left(\frac{\partial v_z}{\partial r} + \frac{\partial v_r}{\partial z}\right) = 0$, where $\tilde{\eta}$ is the kinematic viscosity of the shell and is related to the surface viscosity η by $\eta = d \cdot \tilde{\eta}$. Neglecting $\partial v_z/\partial r$ means that v_r is approximately z independent, thus $v_r = G(t)/r$. The radial component of the hydrodynamic stress tensor is therefore:

$$\tilde{\sigma}_{rr} = -p + 2\tilde{\eta}\frac{\partial v_r}{\partial r} = -p - \frac{2\tilde{\eta}G(t)}{r^2} \tag{9}$$

where p is the pressure field in the shell that enters the Navier-Stokes equation. This hydrodynamic stress tensor, together with the boundary conditions at the circumference of the hole $\tilde{\sigma}_{rr}(r=R) = \frac{T}{R \cdot d}$ and at infinity $\tilde{\sigma}_{rr}(r \to \infty) \cdot d = \sigma$, determine $p \cdot d = \sigma$ and $\frac{R^2}{2\eta}\left(\sigma - \frac{T}{R}\right) = G(t)$, so that $v_r(r=R) = G(t)/R$.

However, the velocity at the circumference of the hole $v_r(r=R)$ is equal to the rate of change of the hole radius $v_r(r=R) = \dot{R}$, thus:

$$\dot{R} = \frac{R}{2\eta}\left(\sigma - \frac{T}{R}\right) \tag{10}$$

which describes the hole growth/healing due to a surface tension σ and a line tension T.

Outflow dynamics

On the scale of the entire shell, the curvature of the shell must be taken into account since it induces a pressure gradient between its two sides, as described by Young-Laplace law. In the presence of a hole, this pressure gradient drives outflow; the outflow decreases the volume and combined area A of the shell. Reduction of the shell area increases the packing density of molecules, which was (before nucleation of the hole) lower than its equilibrium value (due to the constriction), so that the lateral stresses and strains are relieved.

To account for the evolution equation of the combined area A due to outflow, which is determined by the hole radius R and pressure gradient Δp, we again use low Reynolds number hydrodynamics, where now $\vec{v}$ refers to the velocity of the solvent phase of the inner solution and the pressure p now refers to the pressure field inside the high-concentration, polymer solution. This time, the viscosity is not that of the shell but is the kinematic viscosity η_s of the solvent phase of the polymer solution. In the model of case I, a channel forms due to solvent phase flow in the dense, polymer phase. The channel is modeled by a tube of radius R and a contour length of d^*, which is greater than the actual shell thickness d and the hole radius R. In the limit of low Reynolds number, the flow is laminar, meaning that the fluid flow in parallel layers that do not mix. We again work in a cylindrical coordinate system, in which the axis of symmetry of the hole is the $\hat{z}$ axis and $z = 0$ characterizes the midplane of the effective cylinder. The equations governing the flow are the Navier-Stokes equation:

$$\nabla p = \eta_s \nabla^2 \vec{v} \tag{11}$$

and the incompressibility condition, which for laminar, cylindrically symmetric flow ($v_\theta =$

$v_r = 0$ and v_z, p are θ independent) becomes:

$$\begin{aligned} \nabla \cdot \vec{v} &= \frac{\partial v_z}{\partial z} = 0 && (12) \\ \frac{\partial p}{\partial r} &= 0 && (13) \\ \frac{\partial p}{\partial z} &= \eta_s \left(\frac{1}{r} \frac{\partial}{\partial r} \left(r \frac{\partial v_z}{\partial r} \right) + \frac{\partial^2 v_z}{\partial z^2} \right) && (14) \end{aligned}$$

The boundary conditions we use for the velocity field are no-slip boundary conditions on the inner walls of the channel, which are $v_z\left(r = R, z\right) = v_r\left(r = R, z\right) = 0$. For the pressure, in the absence of end effects (applicable when $d^* \gg R$) the boundary conditions are set by the pressure gradient across the membrane (the pressure outside the shell is our reference and is set to zero): $p\left(r, z = 0\right) = -\Delta p$ and $p\left(r, z = d^*\right) = 0$. The solution of these equations with the specified boundary conditions is:

$$\begin{aligned} p\left(z\right) &= \Delta p \left(\frac{z}{d^*} - 1 \right) && (15) \\ v_z &= \frac{\Delta p}{4 \eta_s d^*} \left(R^2 - r^2 \right) && (16) \end{aligned}$$

The total outflow Q is calculated by integration of the velocity v_z over the area of the hole:

$$Q = \int_0^R 2\pi r dr \frac{\Delta p}{4 \eta_s d^*} \left(R^2 - r^2 \right) = \frac{\pi \Delta p R^4}{8 \eta_s d^*} \quad (17)$$

The pressure difference Δp is related to the surface tension by force balance across the shell (Young-Laplace law). Force balance dictates $\nabla \cdot \tilde{\sigma} = 0$ ($\tilde{\sigma}$ is again the three-dimensional stress tensor); in a spherical coordinate system, in which the origin is the center of the ruptured hemisphere the force balance equation becomes

$$\frac{\partial \tilde{\sigma}_{rr}}{\partial r} + 2 \frac{\tilde{\sigma}_{rr}}{r} - \frac{1}{r} \left(\tilde{\sigma}_{\theta\theta} + \tilde{\sigma}_{\phi\phi} \right) = 0 \quad (18)$$

where $\tilde{\sigma}_{\theta\theta} = \tilde{\sigma}_{\phi\phi} = \sigma / d$ (the surface tension divided by the shell thickness) which is constant throughout the thin shell. The stress boundary conditions are $\tilde{\sigma}_{rr}\left(r = R_c\right) = -\Delta p$ and $\tilde{\sigma}_{rr}\left(r = R_c + d\right) = 0$, where R_c is the radius of the hemisphere (and the constriction cross section) and d is the actual thickness of the shell. Multiplying the force balance Eq. 18

by r^2 and integrating between R_c and $R_c + d$, gives the relation:

$$\Delta p \approx \frac{2\sigma}{R_c} \tag{19}$$

which becomes accurate for a thin shell where $d \ll R_c$. Substituting this relation in Eq. 17 results in:

$$Q = \frac{\pi\sigma R^4}{4\eta_s R_c d^*} \tag{20}$$

The outflow decreases the volume V_s of the deformed shell and causes the length L of the cylindrical part of the shell (see Fig. 1B) to decrease. This can be related to the change in the combined area A in the following way:

$$-Q = \frac{dV_s}{dt} = \frac{d}{dt}\left(\frac{4\pi R_c^3}{3} + \pi R_c^2 L\right) = \pi R_c^2 \frac{dL}{dt} \tag{21}$$

$$\frac{dA}{dt} = \frac{d}{dt}\left(4\pi R_c^2 + 2\pi R_c L\right) = 2\pi R_c \frac{dL}{dt} = -\frac{2Q}{R_c} \tag{22}$$

Substituting Eq. 20 in the relation above, results in an equation that describes the time evolution of the combined area A:

$$\frac{dA}{dt} = -\frac{\pi^2\sigma R^4}{2\eta_s A_c d^*} \tag{23}$$

where $A_c = \pi R_c^2$ is the cross sectional area of the constriction. Together with Eq. 10 for the dynamics of the hole size, Eq. 23 forms a complete set of coupled equations that describe the dynamics of the rupture in the fluid-like regime. Using linear elasticity relation $\sigma = E\varepsilon$ the equation becomes:

$$\frac{dR}{dt} = \frac{E}{2\eta} R\left(\varepsilon - \frac{T}{ER}\right) \tag{24}$$

$$\frac{dA}{dt} = -\frac{\pi^2 R^4 E}{2\eta_s A_c d^*}\varepsilon \tag{25}$$

Dimensionless form of the equations

This set of equation is non-linear and cannot in general be solved analytically. However, solutions can be obtained in approximate manner using perturbation expansions of the variables, which first requires identification of the small parameters. This can be done by transformation of the equations to dimensionless form. We thus rescale the hole radius R by its initial

radius R_i, the shell and constriction areas A and A_c by A_u and the time t by the typical viscoelastic timescale $\tau = \eta/E$. This results in the following set of equations:

$$\frac{d\tilde{R}}{d\tilde{t}} = \frac{1}{2}\tilde{R}\left(\varepsilon - \beta\frac{1}{\tilde{R}}\right) \tag{26}$$

$$\frac{d\tilde{A}}{d\tilde{t}} = -\frac{\rho^2\tilde{R}^4}{2\delta\tilde{A}_c}\varepsilon \tag{27}$$

where the parameters β, ρ and δ are $\frac{T}{ER_i}$, $\frac{\pi R_i^2}{A_u}$ and $\frac{\eta_s d^*}{\eta}$ respectively. henceforth, for brevity the tilde signs will be omitted from the rescaled variables. The theory is analyzed in the linear regime, so that the difference between the undeformed nuclear radius R_n and the constriction cross sectional radius R_c is small, i.e $R_n - R_c \ll R_n$. The radii R_n and R_c are related to the undeformed shell area and the constriction cross sectional area by $\pi R_c^2 = A_c$ and $4\pi R_n^2 = A_u$. Therefore $\tilde{A}_c = \frac{A_c}{A_u} = \frac{1}{4}\left(1 - \frac{R_n - R_c}{R_n}\right)^2 = \frac{1}{4} + O\left(\frac{R_n - R_c}{R_n}\right)$. However, in the linear elastic regime, the strain ε is also a small parameter; therefore the deviation of $\tilde{A}_c$ from $\frac{1}{4}$ is higher order in small terms, so that to leading order $\tilde{A}_c$ can be replaced by $\frac{1}{4}$. To linear order in ε the set of equations becomes:

$$\frac{dR}{dt} = \frac{1}{2}R\left(\varepsilon - \frac{\beta}{R}\right) \tag{28}$$

$$\frac{dA}{dt} \approx -\frac{2\rho^2 R^4}{\delta}\varepsilon \tag{29}$$

We further rewrite this using the strain ε, which is a variable which is more physical than the combined area and thus replace A by ε. The lateral strain ε is the ratio of the excess area to the undeformed area A_u and can therefore be written, in non-rescaled variables as $\varepsilon = \frac{A - \pi R^2 - A_u}{A_u}$ or in rescaled variables $\varepsilon = A - \rho R^2 - 1$. Therefore, the time derivative of the lateral strain is

$$\frac{d\varepsilon}{dt} = \frac{dA}{dt} - 2\rho R\frac{dR}{dt} = -\left(1 + \frac{2\rho R^2}{\delta}\right)\rho R^2\varepsilon + \rho R\beta \tag{30}$$

For the biologically relevant values of the initial hole radius of $R_i = 25$nm, which is of the order of the NPC channel size, and the undeformed shell radius of the order of the radius of the nucleus $R_n \approx 3\mu$m , $\rho \approx 1.73 \cdot 10^{-5}$. The value of the parameter $\delta = \frac{\eta_s d^*}{\eta}$ depends on the value of d^*. The equivalent three-dimensional, kinematic viscosity of the lamina (which equals η/d where d is the lamina thickness) is of the order of one kPa $\cdot$ s [1] (we assume that the contribution of the bilayers to the mechanical properties of the NE is small compare

to the lamina); therefore the biologically relevant value of the ratio $\eta_s d/\eta$ is of the order 10^{-6} if η_s is taken to be similar to the kinematic viscosity of water (10^{-3} Pa $\cdot$ s). Choosing $d^*/d \approx 10 - 100$ to account for the tortuosity of the channel, we get $\delta \approx 10^{-5} - 10^{-4}$ and $\rho/\delta \approx 1 - 0.1$. Multiplying this by $\left(\frac{R}{R_i}\right)^2$, which can be much greater than unity when the rupture grows to its maximal size, we find $\frac{2\rho R^2}{\delta} > 1$. Thus, the evolution of the strain can be approximated by

$$\frac{d\varepsilon}{dt} = -\frac{2\rho^2 R^4}{\delta}\varepsilon + \rho R\beta \tag{31}$$

it should be stressed that this approximated form is more accurate when R is close to its maximal size, for $R \approx 1$ Eq. 30 should be used.

For completeness, we estimate in this subsection the value of the parameter β for the model of the lamina as a viscoelastic shell. To estimate β, we start by considering the origin of the line tension. In a coarse-grained view, the bulk of the shell is more hydrophobic than its surfaces (this is the driving force for the creation of the shell in aqueous solution). Thus, hole nucleation creates interface between the hydrophilic solvent and the hydrophobic bulk of the shell; this interface is thermodynamically unfavorable and drives bending of the shell around the circumference of the hole in order to eliminate this interface (see Fig 3. in [2]). This bending energy is results in a line tension, which is the energy of creating unit length of that interface. The bending energy per unit area of the shell is $f_B = \frac{1}{2}K\left(\kappa_1 + \kappa_2\right)^2$, but for bending around the hole one curvature is much larger than the other $\kappa_1 = \frac{2}{d} \gg \frac{1}{R} = \kappa_2$ (d is the shell thickness) so that $f_B = \frac{1}{2}K\left(\frac{2}{d}\right)^2$. The bending modulus K of a plate can be calculated using the equation $K = \frac{\tilde{E}h^3}{12(1-\nu^2)}$ where h is the plate thickness, $\tilde{E}$ and ν are the three-dimensional Young and Poisson moduli respectively [3]. Since the shell folds over itself, it can be viewed as a folded plate, thus $h = d/2$, and $\nu = 1/2$ due to three-dimensional membrane incompressibility. Therefore

$$T = d \cdot f_b = \frac{d\tilde{E}\left(\frac{d}{2}\right)^3}{24\left(1 - \left(\frac{1}{2}\right)^2\right)}\left(\frac{2}{d}\right)^2 = \frac{\tilde{E}d^2}{36} \tag{32}$$

It is important to note that the modulus $\tilde{E}$ that appears above is the three-dimensional Young's modulus, not the two-dimensional Young's modulus E. However, we expect the two to differ by a factor of the order of d, therefore we approximate $T = Ed/36$ in this subsection.

β equals (by definition) to $\frac{T}{ER_i} = \frac{d}{36R_i} \approx \frac{1}{72}$ ($d \approx 14nm$ [4]).

Perturbation analysis and estimate of maximal hole size R_m

The dynamics of the hole radius R and the combined shell area A are determined by the equations 28 and 29:

$$\frac{dR}{dt} = \frac{1}{2}R\left(A - \rho R^2 - 1 - \frac{\beta}{R}\right) \quad (33)$$

$$\frac{dA}{dt} = -2\alpha R^4\left(A - \rho R^2 - 1\right) \quad (34)$$

where $\alpha = \rho^2/\delta$. The dynamics of the hole growth at short times is determined by the value of α and there are two asymptotic limits of interest:

1. Outflow-driven dynamics: In this limit, the majority of the lateral strains due to the constriction are relieved by the outflow of the internal fluid. This limit is characterized by large initial holes (i.e., ρ is relatively large) and small effective dissipation length (i.e., δ is relatively small), which corresponds to values of α which are large $\alpha \equiv \frac{\rho^2}{\delta} \gg 1$. We now follow the perturbation analysis of this limit, beginning with an expansion of $R(t)$ and $A(t)$ as power series in the small parameter $1/\alpha$:

$$R = R^0 + \frac{1}{\alpha}R^1 + O\left(\frac{1}{\alpha^2}\right) \quad (35)$$

$$A = A^0 + \frac{1}{\alpha}A^1 + O\left(\frac{1}{\alpha^2}\right) \quad (36)$$

Rewriting the equations 33 and 34 so that the small parameter $1/\alpha$ appears instead of α gives:

$$\frac{dR}{d\tilde{t}} = \frac{1}{2\alpha}R\left(A - 1 - \rho R^2 - \frac{\beta}{R}\right) \quad (37)$$

$$\frac{dA}{d\tilde{t}} = -2R^4\left(A - 1 - \rho R^2\right) \quad (38)$$

where $\tilde{t} = \alpha t$. Substituting the expansions of R and A and matching the zeroth order terms give:

$$\frac{dR^0}{d\tilde{t}} = 0 \Rightarrow R^0 = 1 \quad (39)$$

$$\frac{dA^0}{d\tilde{t}} = -2\left(A^0 - 1 - \rho\right) \quad (40)$$

so that (the initial condition for A^0 is $A^0\left(\tilde{t}=0\right)=1+\varepsilon_0$)

$$A^0 = 1+\rho+\left(\varepsilon_0-\rho\right)e^{-2\tilde{t}} \tag{41}$$

For $\tilde{t} \ll 1/2$, the exponent in Eq. 41 can be linearized; this gives:

$$A^0 \;=\; 1+\varepsilon_0-2\left(\varepsilon_0-\rho\right)\tilde{t} \tag{42}$$

In the other limit, the exponent in Eq. 41 is very small, therefore $A^0 \approx 1+\rho$. This means that the lateral strain and stresses are now fully relieved, which corresponds to the regime of hole closing. The dynamics of hole closing is found by calculating the first order correction for R, again by matching orders:

$$\frac{dR^1}{d\tilde{t}} \;=\; \frac{1}{2\alpha}\left(A^0-1-\rho\right)-\frac{1}{2\alpha}\beta \tag{43}$$

for short times $\tilde{t} \ll 1/2$ (hole growth) :

$$\frac{dR^1}{d\tilde{t}} \;=\; \frac{1}{2\alpha}\left(A^0-1-\rho\right)-\frac{1}{2\alpha}\beta \tag{44}$$

$$R^1 \;=\; \frac{\left(\varepsilon_0-\rho-\beta\right)}{2\alpha}\tilde{t}-\frac{1}{2}\left(\varepsilon_0-\rho\right)\frac{\tilde{t}^2}{\alpha} \tag{45}$$

and for long times $\tilde{t} \gg 1/2$ (hole shrinking):

$$\frac{dR^1}{d\tilde{t}} \;\approx\; -\frac{1}{2\alpha}\beta \tag{46}$$

$$R^1 \;=\; C-\frac{1}{2}\beta t \tag{47}$$

where C is an integration constant that can be calculated from matching the two regimes.

2. Hole growth-driven dynamics: In this limit, the majority of the lateral strains are relieved by the growth of the hole. This limit is characterized by small initial holes (i.e., ρ is relatively small) and large effective dissipation length (i.e., δ is relatively large), corresponding to values of $\alpha \equiv \frac{\rho^2}{\delta} \ll 1$. Expanding R and A in in the small parameter α:

$$R \;=\; R^0+\alpha R^1+O\left(\alpha^2\right) \tag{48}$$

$$A = A^0 + \alpha A^1 + O\left(\alpha^2\right) \tag{49}$$

Using this equation, equations 33 and 34 give, to zeroth order:

$$\frac{dA^0}{dt} = 0 \Rightarrow A^0 = 1 + \varepsilon_0 \tag{50}$$

so that

$$\frac{dR^0}{dt} = \frac{1}{2}\left(-\left(R^0\right)^3 \rho + \varepsilon_0 R^0 - \beta\right) \tag{51}$$

For short time when R^0 is of order unity, we find in the limit that $\rho \ll \varepsilon_0 - \beta$

$$R^0 = \frac{\beta}{\varepsilon_0} + \left(1 - \frac{\beta}{\varepsilon_0}\right) e^{\frac{1}{2}\varepsilon_0 t} \tag{52}$$

The hole radius of course does not grow indefinitely but is bounded due to the contribution of the $(R^0)^3$ term in Eq. 51. The maximal hole radius can be calculated by searching for the steady state $\frac{dR^0}{dt} = 0$, which results in a polynomial equation of the third degree $(R^0)^3 \rho - \varepsilon_0 R^0 + \beta = 0$; the maximal value of R^0 is the largest real root of the three, which is equal to $\sqrt{\frac{\varepsilon_0}{\rho}} - \frac{\beta}{2\varepsilon_0}$ to first order in β. In the absence of outflow (zeroth order), the maximal hole radius is stable; this is the maximal hole radius in case II (for nucleoplasm as a homogenous viscous fluid) in which outflow is negligible during the exponential growth regime. Addition of slow outflow relieves some of the lateral strains and causes the hole to shrink. Since the lateral strain $\varepsilon = A - 1 - \rho R^2$ is close to zero when R is near its maximal value, Eq. 28 can be written approximately as $\frac{dR}{dt} = -\frac{\beta}{2}$ right after the hole reaches its maximal value. Therefore, the dependence of the hole size on time in this regime is approximately a linear function of time with a slope of $-\frac{\beta}{2}$. However, in the case that the effective dissipation length is too high, outflow will not mitigate the growth of the lateral strain ($\rho\beta R$ is not small compared to $-\left(1 + 2\rho R^2/\delta\right)\rho R^2 \varepsilon$ in 30). This in turn will slow the rate of hole radius decrease, which will return to the value of $-\frac{\beta}{2}$ for a small enough hole, since $\frac{1}{2}R\varepsilon$ will again be negligible compared with $-\frac{\beta}{2}$ in Eq. 28. In this limit, we predict a step-like bump in the dependence of the hole radius on time, which slightly slows the average shrinking rate of the hole. Numerical solutions of the equations over a wide range of effective dissipation lengths verify our prediction of the late-time behavior of the hole radius.

Estimate of the maximal hole radius

Up to this point, the early and late time dynamics of the hole radius have been calculated analytically for different asymptotic regimes. However, in order to fully characterize the dynamics, the transition between the early and late time regimes, or equivalently the maximal hole radius, must be determined. The time at which the transition (or maximal hole radius) occurs is derived from an identity as follows: Multiplying Eq. 29 by $-\frac{1}{4}\frac{\delta}{\rho^2}$ gives

$$-\frac{1}{4}\frac{\delta}{\rho^2}\frac{dA}{dt} = \frac{1}{2}R^4\left(A-\rho R^2-1\right) \tag{53}$$

Next, multiplying Eq. 28 by R^3

$$\frac{1}{4}\frac{d\left(R^4\right)}{dt} = \frac{1}{2}R^4\left(A-\rho R^2-1\right)-\frac{\beta}{2}R^3 \tag{54}$$

and substituting Eq. 53 into Eq. 54 gives

$$\frac{1}{4}\frac{d\left(R^4\right)}{dt} = -\frac{1}{4}\frac{\delta}{\rho^2}\frac{dA}{dt}-\frac{\beta}{2}R^3 \tag{55}$$

Integrating this identity above between the limits of $t=0$ and $t=t_f$ (the time in which the hole closes), using the initial and final conditions$R\left(t=0\right)=1, R\left(t=t_f\right)=0, A\left(t=0\right)=1+\varepsilon_0$ and $A\left(t=t_f\right)=1$ gives the identity:

$$\int_0^{t_f} R^3 dt = \frac{1}{2\beta}+\frac{1}{2\beta}\frac{\varepsilon_0\delta}{\rho^2} \tag{56}$$

It is important to remark that the final condition $A\left(t=t_f\right)=1$ is approximate since in principle, residual strains after healing are possible. However, in the range of parameters which are biological relevant the residual strain is negligible.

The identity in Eq. 56 serves as a constraint that can be used to approximate the transition time between the growth and hole closing regimes. We approximate the hole radius as a function of time to be a piecewise function, where in each regime it is characterized by the asymptotic early and late time dynamics as respectively calculated in equations 52 and 47 (the second applicable to both hole-growth and outflow-driven dynamics); the transition time, or the time at which the hole reaches its maximal radius, R_m can be found using Eq.

56. Denoting the transition time by t_m we split the integral into two regimes:

$$\int_0^{t_f} R^3 dt \;=\; \int_0^{t_m} R^3 dt + \int_{t_m}^{t_f} R^3 dt \tag{57}$$

The late-time ($t > t_m$) dependence of the hole radius in time is approximately $R(t) = R_m - \frac{\beta}{2}(t - t_m)$. Substituting this dependence into the second integral in the right hand side of 57, using $R(t_f) = R_m - \frac{\beta}{2}(t_f - t_m) = 0 \Rightarrow t_f - t_m = \frac{2R_m}{\beta}$ gives:

$$\int_{t_m}^{t_f} R^3 dt \;=\; \int_{t_m}^{t_f} \left(R_m - \frac{\beta}{2}(t - t_m)\right)^3 dt = \int_0^{\frac{2R_m}{\beta}} \left(R_m - \frac{\beta}{2}t'\right)^3 dt' = \frac{1}{2\beta}R_m^4 \tag{58}$$

Therefore, from equations 56, 57 and 58 it follows that

$$2\beta \int_0^{t_m} R^3 dt = 1 + \frac{\varepsilon_0 \delta}{\rho^2} - R_m^4 \tag{59}$$

For the case of hole-growth driven dynamics, which are characterized by $\frac{\delta}{\rho^2} \gg 1$, the identity above is approximately

$$R_m^4 + 2\beta \int_0^{t_m} R^3 dt \approx \frac{\varepsilon_0 \delta}{\rho^2} \tag{60}$$

Solving for t from Eq. 52 for the early-time ($t < t_m$) dynamics calculated in this limit,

$$dt \;=\; \frac{2dR}{\varepsilon_0 R - \beta} \tag{61}$$

the second term on the LHS of Eq. 60 becomes

$$\begin{aligned} 2\beta \int_0^{t_m} R^3 dt \;&=\; 2\beta \int_1^{R_m} \frac{2R^3 dR}{\varepsilon_0 R - \beta} \\ &=\; \frac{4\beta}{3\varepsilon_0}\left(\left(R_m^3 - 1\right) + \frac{3}{2}\frac{\beta}{\varepsilon_0}\left(R_m^2 - 1\right) + 3\frac{\beta^2}{\varepsilon_0^2}(R_m - 1) + 3\left(\frac{\beta^3}{\varepsilon_0^3}\right)\ln\left(\frac{R_m - \frac{\beta}{\varepsilon_0}}{1 - \frac{\beta}{\varepsilon_0}}\right)\right) \end{aligned} \tag{62}$$

As mentioned before, we take $\beta = \frac{1}{72}$, therefore $\frac{\beta}{\varepsilon_0} \approx \frac{1}{2}$. Substituting this ratio and the

order of magnitude $R_m \approx 10$ shows that the value of the integral $2\beta \int_0^{t_m} R^3 dt$ is smaller than R_m^4. We therefore neglect the integral so that Eq. 60 is approximately written as

$$R_m = \left(\frac{\varepsilon_0 \delta}{\rho^2}\right)^{\frac{1}{4}} \tag{63}$$

Eq. 63 can be written in dimensional units as $\frac{\pi R_m^2}{A_u} = \left(\varepsilon_0 \frac{\eta_s d^*}{\eta}\right)^{\frac{1}{2}}$, which predicts the ratio of the maximal hole area and the undeformed area (for fixed constriction cross-sectional area). This ratio increases as the square root of the initial strain ε_0, internal polymer solution kinematic viscosity η_s and the dissipation length d^*. ε_0 is the initial strain that drives hole growth, while the strain relief that limits hole growth decreases with increasing η_s or d^*, which limits the outflow and promotes hole growth. The maximal radius also decreases with the shell surface viscosity η, which slows the hole growth, thus allowing more strain relief by outflow.

This is an approximation that is accurate for small β and large ε_0. In conclusion, for hole growth-driven dynamics (relevant to case I in the main text) the hole radius as a function of time is approximated as:

$$R(t) \approx \begin{cases} \frac{\beta}{\varepsilon_0} + \left(1 - \frac{\beta}{\varepsilon_0}\right) e^{\frac{1}{2}\varepsilon_0 t} & t < t_m \\ \left(\frac{\varepsilon_0 \delta}{\rho^2}\right)^{\frac{1}{4}} - \frac{\beta}{2}(t - t_m) & t \geq t_m \end{cases} \tag{64}$$

where $\left(\frac{\varepsilon_0 \delta}{\rho^2}\right)^{\frac{1}{4}} = \frac{\beta}{\varepsilon_0} + \left(1 - \frac{\beta}{\varepsilon_0}\right) e^{\frac{1}{2}\varepsilon_0 t_m}$.

polymer extrusion as a model for chromatin herniation

To estimate the amount of herniated chromatin, we model the nucleoplasm as a fluid-filled network that comprises a high concentration polymer melt (chromatin) immersed in a viscous solution of water and small molecules. Herniation requires bending of the fibers to radii of curvature which are smaller than the size of the hole. For flow rates smaller than $\frac{k_B T}{\eta_s} \approx 5 \frac{\mu m^3}{s}$ (η_s being the kinematic viscosity of the solvent phase which is taken to be the kinematic viscosity of water) and in the absence of active process, the bending of the polymers is driven by thermal fluctuations [5, 6]. An upper bound for the flow rate can be calculated by taking Eq. 20 and replacing all the variables by their maximal values (R_m is taken to be the larger

value predicted in case II). [All parameters in following equation have their true dimensions.]

$$Q < \frac{\pi E \varepsilon_0 R_m^4}{4\eta_s R_c d^*} \approx \frac{(A_d - A_u)^3}{4\pi\tau\delta R_c A_u} \sim 3\frac{\mu m^3}{s} \tag{65}$$

The actual maximal flow rate is expected to be much smaller than this upper bound since ε is close to zero when $R \sim R_m$, so that the condition $Q < \frac{k_B T}{\eta_s} \approx 5\frac{\mu m^3}{s}$ is surely satisfied for system of biological relevance. Thus, the herniation is not convective, but rather is driven by thermal fluctuations. In order to herniate, a polymer chain must bend to a radius of curvature that is smaller or equal to the radius of the hole R, for a length of at least πR such that a hemicircle is formed; otherwise it cannot slide outside of the hole. Due to the short screening length (Debye length) of the electrostatic interactions in the nucleus which we model, which is of the order of few nanometers [7], the inter- and intra-fiber electrostatic interactions can be neglected. Furthermore, for reasons that are not entirely clear, chromatin fibers in the nucleus may not be entangled [8]. Therefore, the prevalence of steric interaction when the polymer chains locally reorganizes in the vicinity of the hole and these interactions can be neglected as well. With these approximations, the minimal energy E_h of the configuration of the polymer chain that allows herniation arises only from bending, and can be written in terms of the persistence length l_p of the polymer (whose exact value for chromatin is unknown since the in-vivo microscopic structure of chromatin fiber is controversial [9]) as $E_h = \pi k_B T l_p/(2x)$ where x is the radius of curvature and T is the temperature.

The rate of polymer extrusion is therefore the sum over possible radii of curvature from 0 to the hole radius R of Boltzmann probabilities of the form $\nu_0 \exp\left(-\frac{\pi}{2} l_p/x\right)$, where ν_0 is a parameter with dimension of inverse time that represents the molecular kinetics and x is the summation variable. Since the exponent is negative and depends on $1/x$, the sum is dominated by the contribution of the term with the largest x. We thus approximate the extrusion rate by $\nu_0 \exp\left(-\frac{\pi}{2} l_p/R\left(t\right)\right)$, where $R\left(t\right)$ is the hole radius. The total amount of extruded polymer is obtained by integration of the above expression over the entire hole growth/healing cycle of the hole. Cases I and II of the dynamics differ in their prediction for the velocity of hole closing and the maximal hole radius R_m. We therefore calculate the amount of extruded polymer for a general case characterized by an exponential hole growth up to radius R_m followed by a decrease of the hole radius with a constant velocity α. [All variables here, including t have their true dimensions.]

$$L_c \;=\; \nu_0 \int_0^{t_f} e^{-\frac{\pi l_p}{2R(t)}} dt = \nu_0 \tau \left(\int_0^{t_m} e^{-\frac{\pi l_p}{2R(t)}} dt + \int_{t_m}^{t_f} e^{-\frac{\pi l_p}{2R(t)}} dt \right) \tag{66}$$

Taking $\beta/\varepsilon_0 < 1$, $\exp\left(-\frac{\pi}{2} l_p / R\left(t\right)\right) \ll 1$ for small $R\left(t\right)$ and using Eq. 64, we find

$$L_c \;\approx\; \frac{\nu_0 \tau}{\alpha} \int_1^{R_m} e^{-\frac{\pi l_p}{2R}} dR \approx \frac{\nu \tau}{\alpha} \left(R_m e^{-\frac{\pi l_p}{2R_m}} + \frac{\pi l_p}{2} \mathrm{Ei}\left(-\frac{\pi l_p}{2R_m} \right) \right) \tag{67}$$

where Ei is the exponential integral function that defined as $\mathrm{Ei}\left(x\right) = \mathcal{P} \int_{-\infty}^{x} \frac{e^t}{t} dt$ (where $\mathcal{P}$ is the principal part).

References

[1] Joe Swift, Irena L Ivanovska, Amnon Buxboim, Takamasa Harada, PC Dave P Dingal, Joel Pinter, J David Pajerowski, Kyle R Spinler, Jae-Won Shin, Manorama Tewari, et al. Nuclear lamin-a scales with tissue stiffness and enhances matrix-directed differentiation. *Science*, 341(6149):1240104, 2013.

[2] Peter J Photos, Harry Bermudez, Helim Aranda-Espinoza, Julian Shillcock, and Dennis E Discher. Nuclear pores and membrane holes: generic models for confined chains and entropic barriers in pore stabilization. *Soft Matter*, 3(3):364–371, 2007.

[3] Lev D Landau and EM Lifshitz. Theory of elasticity, vol. 7. *Course of Theoretical Physics*, 3:109, 1986.

[4] Yagmur Turgay, Matthias Eibauer, Anne E Goldman, Takeshi Shimi, Maayan Khayat, Kfir Ben-Harush, Anna Dubrovsky-Gaupp, K Tanuj Sapra, Robert D Goldman, and Ohad Medalia. The molecular architecture of lamins in somatic cells. *Nature*, 543(7644):261–264, 2017.

[5] Lucie Béguin, Bruno Grassl, Françoise Brochard-Wyart, Mohammed Rakib, and Hervé Duval. Suction of hydrosoluble polymers into nanopores. *Soft Matter*, 7(1):96–103, 2011.

[6] S Daoudi and F Brochard. Flows of flexible polymer solutions in pores. *Macromolecules*, 11(4):751–758, 1978.

[7] Daniel A Beard and Tamar Schlick. Computational modeling predicts the structure and dynamics of chromatin fiber. *Structure*, 9(2):105–114, 2001.

[8] Waltraud G Müller, Dietmar Rieder, Gregor Kreth, Christoph Cremer, Zlatko Trajanoski, and James G McNally. Generic features of tertiary chromatin structure as detected in natural chromosomes. *Molecular and Cellular Biology*, 24(21):9359–9370, 2004.

[9] Kazuhiro Maeshima, Saera Hihara, and Mikhail Eltsov. Chromatin structure: does the 30-nm fibre exist in vivo? *Current opinion in cell biology*, 22(3):291–297, 2010.